

Qubit Mapping and Routing tailored to Advanced Quantum ISAs: Not as Costly as You Think

Zhaohui Yang
The Hong Kong University of
Science and Technology

Xiangyu Ren
University of Edinburgh
Edinburgh, United Kingdom

Dawei Ding
Tsinghua University
Beijing, China

Kai Zhang
Tsinghua University
Pengcheng Laboratory

Yingjian Liu
Leiden University
Leiden, The Netherlands

Jianxin Chen*
Tsinghua University
Beijing, China

Xinyang Tian
Tsinghua University
Beijing, China

Yunfeng Li
The University of Hong Kong
Hong Kong

Yuan Xie
The Hong Kong University of
Science and Technology

Abstract

Qubit mapping/routing is a critical stage in compilation for both near-term and fault-tolerant quantum computers, yet existing scalable methods typically impose several times the routing overhead in terms of circuit depth or duration. This inefficiency stems from a fundamental disconnect: compilers rely on an abstract routing model (e.g., three-CX-unrolled SWAP insertion) that completely ignores the idiosyncrasies of native gates supported by physical devices.

Recent hardware breakthroughs have enabled high-precision implementations of diverse instruction set architectures (ISAs) beyond standard CX-based gates. Advanced ISAs involving gates such as \sqrt{i} SWAP and ZZ(θ) gates offer superior circuit synthesis capabilities and can be realized with higher fidelities. However, systematic compiler optimization strategies tailored to these advanced ISAs are lacking.

To address this, we propose CANOPUS, a unified qubit mapping/routing framework applicable to diverse quantum ISAs. Built upon the canonical representation of two-qubit gates, CANOPUS centers on qubit routing to perform deep co-optimization in an ISA-aware approach. CANOPUS leverages the two-qubit canonical representation and the monodromy polytope to model the synthesis cost for more intelligent SWAP insertion during the routing stage. We also formalize the commutation relations between two-qubit gates through the canonical form, providing a generalized approach to commutativity-based optimizations. Experiments show that CANOPUS consistently reduces routing overhead by 15%-35% compared to state-of-the-art methods across different ISAs and topologies. Our work also presents a coherent method for co-exploration of program patterns, quantum ISAs, and hardware topologies. We have for the first time demonstrated that advanced quantum ISAs can be efficiently utilized within a unified routing framework, paving the way for more effective co-design of quantum software and hardware.

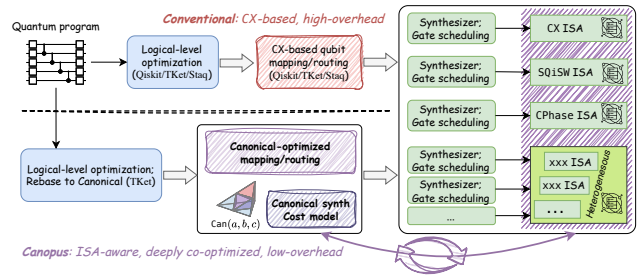


Figure 1. Compilation workflows by means of conventional approaches (top) and CANOPUS (bottom) targeting diverse quantum ISAs. CANOPUS integrates the synthesis cost model (monodromy polytopes within the Weyl chamber) to consider backend ISA properties during the routing stage. CANOPUS routing operates in the 2Q canonical representation while the specific synthesis is completed by the backend synthesizer.

1 Introduction

Quantum computing is a revolutionary computational paradigm leveraging quantum mechanical principles such as superposition and entanglement of qubit states [47]. It has grown rapidly in recent decades due to the potential speedup in tasks such as integer factorization [58], solving linear equations [23], and simulation of quantum systems [41].

Holistic benchmarks of quantum computers such as quantum volume [16] are predicated on concurrent advancements in both hardware and software. Recently, numerous systematic techniques regarding compiler optimization and architectural support have been presented to push the limit of hardware performance. Quantum compilers play a pivotal role in this process, translating high-level programs into executable single-qubit (1Q) and two-qubit (2Q) gates on realistic quantum hardware. This typically involves several stages: (1) compiling programs into basic quantum gates, (2) performing hardware-agnostic (logical-level) circuit optimization, (3) resolving backend topology constraints via qubit placement and routing, and (4) converting circuits to native gates for

*Corresponding author. Email: chenjianxin@tsinghua.edu.cn.

final optimization and scheduling. The primary goal of compiler optimization is to lower the 2Q gate count and circuit depth while resolving backend constraints, with a particular emphasis on 2Q gates due to their significantly higher error rates compared to 1Q gates.

For mainstream quantum platforms such as superconducting qubits [33], 2Q gates can only operate between nearest-neighbor physical qubit pairs (e.g., Google’s devices with 2D square topology [4], IBM’s devices with 2D heavy-hex topology [10]). Consequently, qubit placement and routing is crucial for resolving this connectivity constraint by dynamically remapping logical qubits to physical ones by inserting SWAP gates acting on adjacent physical qubit pairs. This introduces a routing overhead that typically increases the gate count and circuit depth by a factor of 2x-4x relative to the pre-mapped circuits when using state-of-the-art (SOTA) scalable routing methods [38, 40, 69, 73]. Therefore, mitigating this routing overhead remains a central and long-standing challenge in compiler optimization.

Most studies on qubit routing rely on a simplified routing model, where circuit cost is quantified by the CX-based gate count and circuit depth while each SWAP gate is unrolled into three CX gates according to the textbook pattern $\text{SWAP}_{q_0, q_1} = \text{CX}_{q_0, q_1} \text{CX}_{q_1, q_0} \text{CX}_{q_0, q_1}$. However, this CX-centric view is misaligned with the physical reality of modern quantum devices. Although quantum algorithms are typically expressed in terms of CX gates, the underlying hardware may not execute native CX-equivalent gates, nor does this gate/circuit cost quantification method accurately reflect the true operational cost. Indeed, beyond the native support for CX-equivalent gates (e.g., CZ [33], Cross-Resonance [56], Mølmer-Sørensen [7]), modern quantum hardwares increasingly feature diverse native 2Q basis gates in recent years. These alternative basis gates, or the abstracted instruction set architectures (ISAs) can be more powerful than CX-equivalent gates in terms of synthesis capabilities and fidelity of realization, such as \sqrt{i} SWAP [26], the iSWAP-family and CX-family gates [28, 45], and heterogeneous/combinatorial basis gates [45, 50]. With such ISAs, SWAP can be implemented with a lower cost than three CX gates or even be natively realized with high fidelity [12, 46, 63]. Therefore, the simplified routing model completely ignores the backend ISA properties, severely limiting the potential of compiler optimization. Furthermore, the absence of systematic compiler optimization methods across these diverse (even complex, heterogeneous) ISAs has prevented the community from fully exploiting their power and exploring the rich software-hardware co-design space.

In our work, we propose a unified qubit mapping/routing framework CANOPUS (**C**anonical-**O**ptimized **P**lacement **U**tility **S**uite) tailored to diverse quantum ISAs. Unlike conventional CX-based routing approaches, CANOPUS is fundamentally

ISA-aware. As illustrated in Figure 1, it considers the properties of the target ISA by formulating an appropriate cost model to perform deep co-optimization of routing and synthesis. By means of the canonical 2Q representation [70], CANOPUS fully exploits the synthesis capabilities of the given ISA. This approach demonstrates that advanced ISAs can achieve significantly lower routing overheads than conventional models suggest.

The main ideas of CANOPUS are as follows: ① Considering the subsequent synthesis overhead with native basis gates after the qubit routing stage could unlock significant optimization opportunities. For instance, a SWAP inserted after a 2Q block with the same qubit pair acted on could lead to a better synthesis result when rebased to the backend ISA. ② Expanding the quantum ISA is crucial to boost the performance of real-world quantum applications. For example, the fractional ZZ(θ) gate set widely adopted by hardware vendors (e.g., IBM [27], Quantinuum [54], IonQ [29]) enables more efficient execution of chemistry simulation kernels within which many 2-local Pauli rotations are involved. The combination of CX and iSWAP gates have been demonstrated to benefit stabilizer circuits to protect error-corrected qubit information [71]. ③ The monodromy polytope theory [51] based on the canonical representation of 2Q gates [70] provides a formal, universal, and quantitative description of the 2Q synthesis cost for generic quantum ISAs. This formalism enables unified compiler optimization. With these insights in mind, CANOPUS performs intelligent SWAP insertion during qubit routing to holistically minimize post-mapping circuit cost (in terms of both gate count and depth) given any quantum ISA, thus performing deep routing-synthesis co-optimization and resulting in significantly lower routing overheads. Importantly, although CANOPUS is ISA-aware, it always operates on the canonical-form circuits, and the gate/circuit cost quantification via monodromy polytopes is independent of the specific ISA rebase implementation. Thus CANOPUS offers an LLVM-style optimization.

Experimental results demonstrate that CANOPUS consistently provides 15%-35% reduction (in terms of both gate count and depth) of routing overhead compared to other SOTA methods across representative quantum ISAs, *including the conventional CX ISA*. This cross-ISA comparison also reveals some consistent or program-specific or topology-specific guidelines for hardware-software co-design. Source code and data are available via the Github link. Our work makes the following key contributions:

- ① We utilize the canonical 2Q gate representation and the monodrome polytope to quantify costs of 2Q gates and the overall circuit. This formal approach accurately guides synthesis-routing co-optimization and cross-ISA evaluation.
- ② We formalize the analysis of commutation relations between arbitrary 2Q canonical gates that share one qubit. This offers a generalized commutativity-based optimization mechanism, moving beyond those tailored only for CX gates [39].

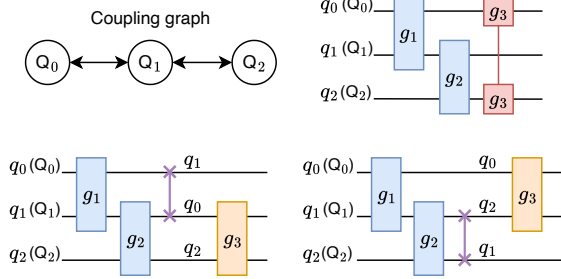


Figure 2. Mapping/routing to resolve topology constraints via SWAP insertion. With the initial mapping $\{q_i : Q_i\}$ (upper right), g_3 is not hardware compliant. Both SWAP_{q_0, q_1} and SWAP_{q_1, q_2} are sufficient to make g_3 executable.

③ We conduct comprehensive experiments across a wide range of real-world benchmarks, hardware topologies, and representative ISAs, showing that CANOPUS consistently reduces routing overhead by 15%-35% compared to SOTA methods. Our results also yield holistic guidelines for the co-design of quantum programs, ISAs, and hardware.

④ We confirm that theoretically expressive ISAs exhibit superior performance to the conventional CX ISA, challenging the conclusions of prior works [31]. We demonstrate some co-design guidelines for ISA-program-topology co-exploration.

⑤ Our case studies, including the real-machine QFT kernel execution and the end-to-end QEC circuit simulation, unequivocally showcase CANOPUS' superiority in both near-term and fault-tolerant applications. For example, on the task of mapping QFT on 1D chain topology, CANOPUS finds the provably optimal routing scheme, surpassing the results previously reported as optimal in prior work [69]; and experiments on IBM's QPUs suggest that CANOPUS leads to an average 2.1x fidelity improvement compared to QISKIT.

2 Background

2.1 Qubit mapping/routing

Real quantum hardware typically have connectivity constraints, whereas algorithms often assume arbitrary interactions. To execute quantum circuits on topology-constrained hardware, logical qubits must first be mapped to physical qubit positions. This is called the initial mapping. In most cases, even an optimal initial mapping cannot guarantee all logical 2Q gates are mapped on physically connected qubit pairs. The common solution is to dynamically change logical-to-physical qubit mappings by inserting SWAP gates, as a SWAP gate exchanges state subspaces of two operand qubits, such that non-adjacent logical qubit states can be moved next to each other. Therefore, the qubit placement and routing compilation stage takes a logical circuit and hardware coupling graph as the input and outputs a transformed circuit within which each 2Q gate, with respect to a qubit mapping, is hardware compliant. An example is depicted in Figure 2.

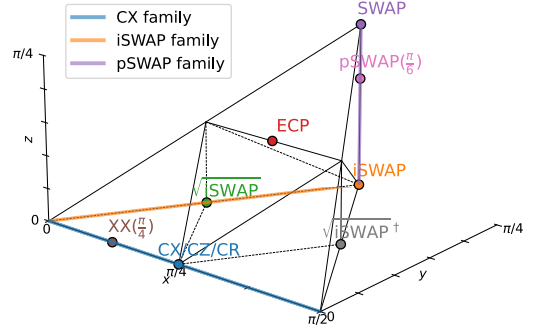


Figure 3. Geometric illustration of canonical gates confined to the Weyl chamber. For visualization convenience, herein the Weyl chamber is confined to $\{\frac{\pi}{4} \geq x \geq y \geq z \geq 0\} \cup \{\frac{\pi}{4} \geq \frac{\pi}{2} - x \geq y \geq z \geq 0\}$, equivalent to the canonical coefficient convention $\{(a, b, c) \mid \frac{1}{2} \geq a \geq b \geq |c|\}$ throughout this paper.

2.2 Canonical description of 2Q gates

Any 2Q gate can be represented by a 4x4 matrix in $\text{SU}(4)$, up to a global phase, with its canonical form defined as:

Definition 1 (Canonical gate). *Any 2Q gate $U \in \text{SU}(4)$ can be expressed by the composition of its unique canonical form*

$$\text{Can}(a, b, c) := e^{-i\frac{\pi}{2}(aXX+bYY+cZZ)}, \frac{1}{2} \geq a \geq b \geq |c| \quad (1)$$

sandwiched by local 1Q gates such that we say U is locally equivalent to the canonical form $\text{Can}(a, b, c)$.

The canonical coefficients (a, b, c) are confined to a tetrahedron known as the *Weyl chamber*, which provides a geometric representation of all local equivalence classes of 2Q gates [70]. Figure 3 visualizes some common 2Q gates. E.g.,

- CX, CZ, and CR are all equivalent to $\text{Can}(\frac{1}{2}, 0, 0)$.
- CX family: $\text{XX}(\theta) \sim \text{YY}(\theta) \sim \text{ZZ}(\theta) \sim \text{Can}(\frac{\theta}{\pi}, 0, 0)$.
- Param-SWAP family: $\text{pSWAP}(\theta) \sim \text{Can}(\frac{1}{2}, \frac{1}{2}, \frac{1}{2} - \frac{\theta}{\pi})$.

In practice, the canonical form is acquired by KAK decomposition [61] and has been widely used [8, 11].

2.3 Gate realization cost on hardware

The transformed circuits via qubit routing will be ultimately converted into basis gates for execution on hardware. Basis gates refer to those natively implemented and calibrated on physical platforms. Typical native gates in superconducting are CR [56], CZ, and iSWAP gates [33]. The realization cost of basis gates involves multiple aspects, including the benchmarked fidelity, gate duration, calibration efficiency, etc. For example, gates with shorter duration are more likely to achieve high fidelity, as qubit decoherence dominates the noise source; although some gate schemes can now implement more basis gates [12, 46], those with simpler pulse control are more likely to be calibrated with high precision, such as the iSWAP family on flux-tunable transmons.

2Q gates that are not natively implemented must be synthesized by native gates. Their realization cost is determined by what basis gates are required for synthesis. For example, any 2Q gate can be minimally synthesized by 3 CX gates, except for $\text{Can}(a, b, 0)$ for which the required CX count is 2. Conventionally, SWAP is regarded as 3 times that of CX realization cost, while it can also be synthesized by “1 CX + 1 iSWAP” or “3 $\sqrt{\text{iSWAP}}$ ” gates. The monodromy polytope theory was proposed to determine the optimal synthesis cost for any 2Q gate given a specific set of basis gates through analysis of local invariants of canonical gates [51]. By this method, the set of gates realizable by a specified number of 2Q gates from the basis set, with arbitrary 1Q gates, corresponds to a polytope within the Weyl chamber. For instance, the polytope for 2 $\sqrt{\text{iSWAP}}$ gates is a tetrahedron confined to $\{1/2 \geq a \geq b + |c|\}$ [26].

3 Motivation

Limitations of conventional qubit routing models.

Conventional qubit routing models are ill-equipped to exploit the versatility of modern quantum hardware. First, whether optimizing for gate count or circuit depth, they typically assume that a SWAP costs 3 CX gates according to the textbook decomposition. This assumption is divorced from hardware reality. For example, a combination of CX and iSWAP is sufficient to realize a SWAP while both CZ (locally equivalent to CX) and iSWAP are natively supported on mainstream superconducting platforms like Google’s Sycamore [4]. Such platforms can even directly implement a high-fidelity SWAP gate, with the pulse duration 1.5 times that of CZ [12]. Thus, SWAP is not as costly as what these previous works on routing assume. Second, while prior works like Liu et al. [39] do assume the cost of a SWAP is context-dependent, their analysis remains confined to the CX-based routing model. By relying on this overly simplistic model, conventional routers cannot accurately predict circuit execution costs and are blind to the significant optimization opportunities offered by richer, more diverse ISAs.

Co-optimization as the key to unlocking the superiority of advanced ISAs. In response to the limitations of the CX-only paradigm, a new generation of sophisticated quantum processors has emerged, featuring advanced ISAs with more powerful basis gates. Notable examples include the $\sqrt{\text{iSWAP}}$ gate proposed by Huang et al. [26], the continuous ZZ(θ) (equivalent to XX(θ), ZX(θ), MS(0, 0, $\theta/2$)) jointly adopted by vendors [27, 29, 54], and selected fractional or heterogeneous basis gates [45]. Despite their theoretical promise for greater synthesis power and noise resilience, these advanced ISAs have largely remained in the proof-of-concept stage, with no systematic framework to harness their full potential in real-world quantum applications.

Prior efforts have been narrowly focused on local 2Q or multi-qubit synthesis tasks [26, 60] or brute-force numerical

optimizations [17, 68]. Such rebase passes are tailored to a specific quantum ISA and fail to provide clear benefits when applied to advanced ISAs in realistic workloads [31]. This has led to a critical question lingering in the community: “Are these more expressive, noise-resilient ISAs actually better?” Recently there have been attempts to harness the properties of advanced ISAs, although through manual and unsophisticated design, such as the $\sqrt{\text{iSWAP}}$ -based routing-synthesis optimization [45] and the CX-iSWAP based routing for defect mitigation [71]. In our work, we highlight that collaborative compiler optimization, especially at the stage following logical-level circuit optimization and followed by the final ISA rebase pass, is a key to fully exploit capabilities of those powerful ISAs: First, high-level algorithms are expressed in the CX representation, which then undergo template-based and peephole optimizations that are highly sophisticated and tailored for CX-based circuit patterns (e.g., commutativity, Clifford equivalence); Second, the gap between the naïve qubit routing model and backend ISA properties apparently leaves a large untapped co-optimization space for both qubit routing and ISA rebase. Thus we are committed to validating this point through a systematic ISA-aware routing framework.

The “Tower of Babel dilemma” for utilizing diverse ISAs. The proliferation of diverse quantum ISAs—from monolithic to complex, heterogeneous basis gate sets supported by various physical platforms—has created a “Tower of Babel dilemma” in the architecture and systems community. Developing bespoke compiler optimizations for each unique hardware backend is unsustainable, leading to the same software fragmentation that we have encountered in classical computing. Consequently, it is important to seek a unified approach that can effectively handle various platform-specific abstractions resembling the LLVM compiler [36]. The recently proposed monodromy polytope theory [51], for example, provides the method for optimal analysis of ISA synthesis capabilities. Specifically regarding the circuit-level compiler optimization, the monodromy polytope with canonical 2Q gate representations offers a unified approach to evaluating circuit cost and modeling routing-synthesis co-optimization. Building on this, CANOPUS offers an elegant and unified solution to the Tower of Babel dilemma at the compiler level.

Coherent cross-ISA, topology, and program pattern co-exploration. Ultimately, the goal of quantum computing systems is not just to optimize software for existing hardware, but to co-design the entire stack—from algorithms to architecture—to build the most efficient system possible. This requires a holistic exploration of a vast and complex design space, asking critical questions like: Which ISA is best suited for a given class of applications (e.g., quantum error correction vs. quantum simulation)? How does the choice of

qubit topology interact with the ISA to affect performance? Answering these questions is currently an ad-hoc, labor-intensive process, hindering systematic progress. Therefore, our work aims to provide the missing piece: a unified and automated framework for this co-exploration. By integrating qubit routing with a formal, ISA-aware synthesis cost model, CANOPUS can systematically evaluate the performance of different program patterns across heterogeneous ISAs and diverse hardware topologies. This enables researchers and hardware designers to make informed, data-driven decisions, accelerating the discovery of optimal co-design points and paving a systematic path toward robust, fault-tolerant quantum computer systems.

4 CANOPUS framework

4.1 Overview

The overall routing procedure of CANOPUS is illustrated in Figure 4. The input circuit is rebased to $\{\text{Can}, \text{U3}\}$ before being fed to the routing pass. All processes operate on the directed acyclic graph (DAG) representation of the circuit. CANOPUS integrates the ISA-specific synthesis cost model into its SWAP search process and determines the best SWAP at each route step. The routing cost is efficiently computed by a formal analysis of 2Q canonical forms, without the ISA rebase step. Thus, the output is still a circuit DAG represented in $\{\text{Can}, \text{U3}\}$ with inserted SWAP gates.

Notably, CANOPUS inherits the basic concepts and data structures introduced in SABRE [38], which is one of the industrial-standard qubit mapping algorithms. Given the input circuit DAG, CANOPUS first attempts to map 2Q gates layer by layer via extracting the front layer F , peeling executable gates and searching SWAP gates to minimize the routing cost according to a heuristic cost function. On the backbone of SABRE, we further introduce several key data structures such as the last mapped layer L and the wire duration records D , to support the efficient implementation of ISA-aware routing and reducing both gate count and depth related routing overhead.

4.2 2Q synthesis cost modeling

As introduced in Section 2.3, given any basis gate set, the synthesis cost of a target 2Q gate can be exactly computed through the monodromy polytopes [51]. This cost (which basis gates are sufficient for synthesis) only depends on the canonical coefficients of the target gate. For example, Figure 5 illustrates various polytopes for the gate set $\{\sqrt{\text{iSWAP}}, \text{ECP}\}$. In practice, the costs of each basis gate are pre-defined, thus the whole polytope helps decide the optimal synthesis scheme we should prioritize with the minimal circuit cost. For example, if $\sqrt{\text{iSWAP}}$ and ECP have the same unit cost, the $\text{SWAP} \sim \text{Can}(\frac{1}{2}, \frac{1}{2}, \frac{1}{2})$ gate realization will prioritize the “ $1\sqrt{\text{iSWAP}} + 1\text{ECP}$ ” combination; if ECP cost is set to be more

than twice that of $\sqrt{\text{iSWAP}}$, the SWAP realization prioritizes the “ $3\sqrt{\text{iSWAP}}$ ” pattern.

4.3 Routing in canonical form

Our ISA-aware routing primarily leverages the mechanism that some inserted SWAP gates can “piggyback” a preceding 2Q gate with the same qubit pair acted on and thus result in lower (even negative) routing overhead than what naïve SWAP synthesis cost may imply. Based on the ISA-specific synthesis cost model, CANOPUS utilizes a holistic heuristic cost function that considers various requirements of qubit routing in a unified, quantitative approach.

As Figure 6(a) shows, every 2Q block within the circuit is consolidated into a single unitary gate and rebased to $\{\text{Can}, \text{U3}\}$. During qubit routing, when a SWAP insertion follows a 2Q gate U acting on the same qubit pair, the actual insertion cost is reflected by the minimal set of basis gates sufficient for synthesizing the composite block $\text{SWAP} \cdot U$, rather than by the cost of the SWAP gate itself (c_{swap}). Specifically, CANOPUS tracks the set of 2Q canonical gates that have no succeeding 2Q gates within the DAG constructed by already routed gates, as the “last mapped layer” L . We define the cost component $c_g = \text{COST}(\text{SWAP} \cdot U) - \text{COST}(U)$ if an inserted SWAP can be “absorbed” by L , while $c_g = c_{\text{swap}}$ if it cannot. We further consider the cost for the circuit depth increment Δ_{depth} during qubit routing, which is evaluated by tracking depth costs (durations) on every qubit wire, recorded as D . Figure 6(b) illustrates that different SWAP insertion patterns may lead to different gate count and depth costs, and thus should be comprehensively considered. Notably, the circuit depth (duration) is quantified with given basis gate costs, i.e., length of the weighted critical path on the circuit DAG. The detailed heuristic cost function in CANOPUS is defined as:

$$H = w_g c_g + w_d \Delta_{\text{depth}} + (\Delta_{\text{Avg}\{\text{dist}[i,j]\}_F} + k_E \Delta_{\text{Avg}\{\text{dist}[i,j]\}_E}) c_{\text{swap}}, \quad (2)$$

where w_g and w_d are the weight factors for the gate count and depth cost components, respectively. The last term reflects the original heuristic cost $H_{\text{SABRE}} = \text{Avg}\{\text{dist}[i,j]\}_F + k_E \text{Avg}\{\text{dist}[i,j]\}_E$ in SABRE [38], while used in a unified approach accompanied with the other cost components in CANOPUS. Specifically, H_{SABRE} refers to the average distance between physical qubits mapped to demanded logical interactions in the front layer F and the extended set E (lookahead mechanism). Here we use the “differential” average distance after inserting a SWAP candidate, then multiply it by the c_{swap} to reflect on average how an inserted SWAP can reduce the distance between each physical qubit pair, with the negative distance-cost increment quantified in the basis. Furthermore, the decay factor in SABRE is not needed anymore, as the c_g and Δ_{depth} guide more accurate co-optimization. Therefore, each cost component in Equation (2) refers to

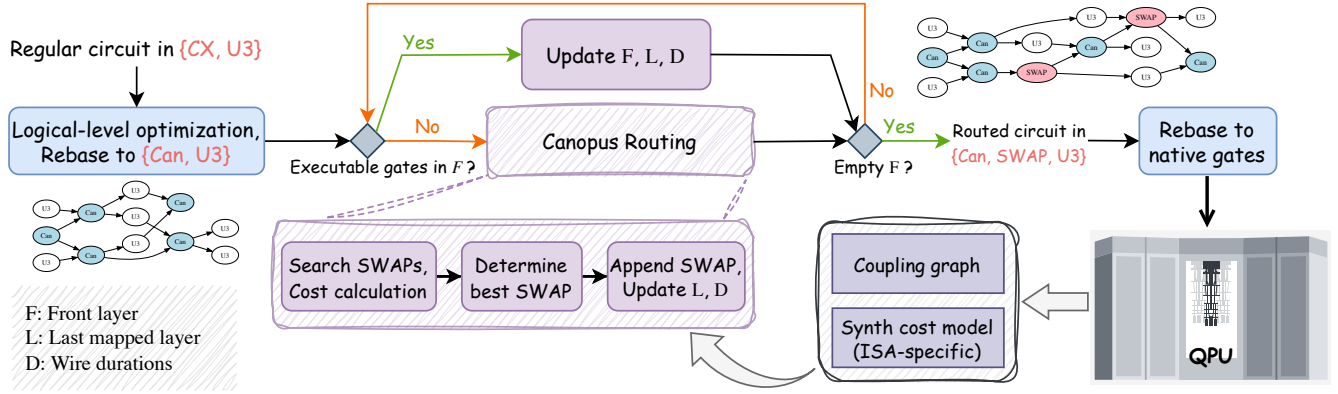


Figure 4. Overview of the CANOPUS framework.

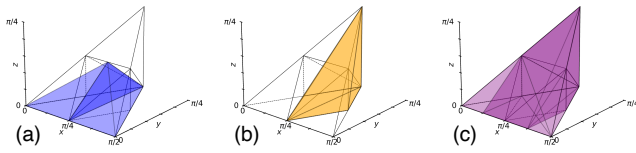


Figure 5. Synthesis coverage for $\{\sqrt{i}\text{SWAP}, \text{ECP}\}$ gate set. The trivial points ($\sqrt{i}\text{SWAP}$ and ECP themselves) are not shown in this figure. 2Q coverage regions correspond to those that require (a) 2 $\sqrt{i}\text{SWAP}$ gates or 2 ECP gates; (b) 1 $\sqrt{i}\text{SWAP}$ + 1 ECP; (c) 3 gates (3 $\sqrt{i}\text{SWAP}$, 3 ECP, 2 $\sqrt{i}\text{SWAP}$ + 1 ECP, etc.) from this gate set for synthesis, respectively.

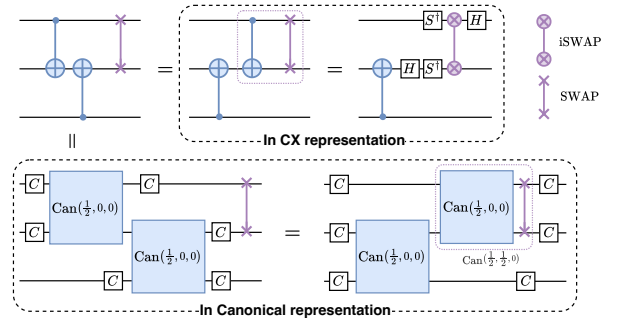
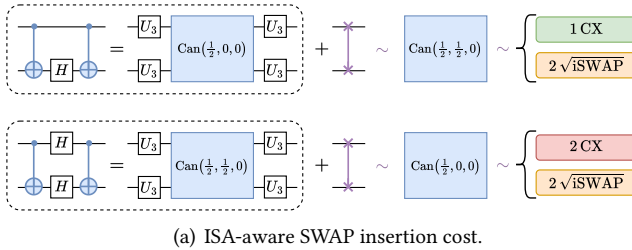
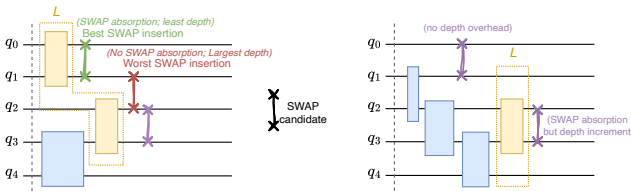


Figure 7. Canonical gate representation enables easily capturing commutative relations within real-world circuits. Commutativity within CX chain can be formally captured without tracking either’s control and target qubit positions. In the bottom subfigure C indicates the 1Q Clifford gate.



(a) ISA-aware SWAP insertion cost.



(b) SWAP insertion patterns with different gate count and depth costs.

Figure 6. Qubit routing with the canonical 2Q gate representation.

“cost increment”, composing a unified heuristic cost function to reconcile the multifaced routing costs.

4.4 Enhanced optimization via commutation

Previous works have observed that employing the commutativity between CX gates exposes more optimization opportunities for SWAP insertion [39]. However, the commutation pattern they exploit is limited to a pair of CX gates, where they either act on the same control qubit or target qubit. In our findings, the general 2Q gate commutativity can be captured through the canonical form:

Theorem 1 (Canonical gate commutation). *Let $\text{Can}(a, b, c)_{q_0, q_1}$ and $\text{Can}(a', b', c')_{q_1, q_2}$ denote canonical gates acting on qubits (q_0, q_1) and (q_1, q_2) respectively, with an overlapping qubit q_1 . They are commutative if and only if*

$$b = b' = c = c' = 0, \quad (3)$$

that is, when both consist solely of XX rotations.

Detailed proof is provided in Appendix B. Through this formalized commutativity determination, the ordinary CX commutation pattern can be captured without tracking the control and target qubit positions, as shown in Figure 7.

Algorithm 1: Update L when adding a new 2Q gate

```

Input :  $G'$  (Routed DAG),  $\pi$  (current logic-to-physical
          mapping),  $L$  (last mapped layer),  $D$  (wire durations
          for each qubit),  $C$  (commutative pairs within  $L$ )
Output: Updated  $G'$ ,  $L$ ,  $D$ ,  $C$ 

/*  $g$ : resolved logical gate;  $g'$ : routed gate */
1  $g' \leftarrow G'.\text{PUSHBACK}(g, \pi[g.q_0], \pi[g.q_1]);$  //  $g'.q_i = \pi[g.q_i]$ 
2  $d \leftarrow \text{MAX}(D[g'.q_0], D[g'.q_1]) + \text{SYNTHCOST}(g);$ 
3  $D[g'.q_0] \leftarrow d; D[g'.q_1] \leftarrow d;$ 
4 for  $\text{pred} \in G'.\text{PREDECESSORS}(g')$  do
5   if  $\text{IS2QGATE}(\text{pred})$  then
6     if  $\text{ISCOMMUTATIVECANONICALPAIR}(g', \text{pred})$  then
7        $C[(\text{pred}.q_0, \text{pred}.q_1)] \leftarrow (g'.q_0, g'.q_1);$ 
8     else
9        $L.\text{POP}((\text{pred}.q_0, \text{pred}.q_1), \text{NONE});$ 
10       $C.\text{POP}((\text{pred}.q_0, \text{pred}.q_1), \text{NONE});$ 
11   else
12     /*  $\text{pred\_pred}$  must be None or a 2Q gate */
13      $\text{pred\_pred} \leftarrow \text{NEXT}(G'.\text{PREDECESSORS}(\text{pred}));$ 
14     if  $\text{pred\_pred} \neq \text{NONE}$  then
15        $L.\text{POP}((\text{pred\_pred}.q_0, \text{pred\_pred}.q_1), \text{NONE});$ 
16        $C.\text{POP}((\text{pred\_pred}.q_0, \text{pred\_pred}.q_1), \text{NONE});$ 
17    $L[(g'.q_0, g'.q_1)] \leftarrow g';$ 

```

4.5 Scalability and implementation

The overall algorithm framework to implement CANOPUS resembles CANOPUS. To efficiently implement the sophisticated SWAP insertion mechanism in CANOPUS, we develop corresponding core algorithms. Algorithm 1 specifies how the demanded data structures—the last mapped layer L , commutative canonical gate pairs C within L , wire duration record D —will be updated when adding an executable 2Q gate to the routed circuit DAG. Algorithm 2 shows how the wire durations D should be correctly updated when encountering a SWAP insertion that satisfies the canonical gate commutativity optimization opportunity. It is also essential to evaluate the total circuit cost after mapping. Notably, all the computation processes within these algorithms are based on conditional control and operations on hashed data structures, thus with $O(1)$ time complexity introduced. To quantify the synthesis cost computation of a given canonical gate, the computation is to determine which convex polytope its canonical coordinate is located in, which is a highly efficient computation process with linear time complexity. CANOPUS will also cache canonical gate costs it has acquired to avoid repetitive computation. Consequently, the overall scalability of CANOPUS is on par with that of SABRE, ensuring its practical applicability to large-scale circuits.

Algorithm 2: Update D when adding a SWAP gate

```

Input :  $\text{swap}$  (encountered SWAP gate),  $\text{can}$  (canonical
          gate within  $L$  on the same qubits as  $\text{swap}$ ),  $D$ ,  $C$ 
Output: Updated  $D$ 

1 if  $(\text{swap}.q_0, \text{swap}.q_1) \in C$  then
2    $q'_0, q'_1 \leftarrow C[(\text{swap}.q_0, \text{swap}.q_1)];$ 
3   /* Adjust  $D$  by finding matched qubits
4      $q_i \in \{\text{swap}.q_0, \text{swap}.q_1\}$  and  $q'_j \in \{q'_0, q'_1\}$  */
5    $D[q_i] \leftarrow D[q'_j] + \text{SYNTHCOST}(\text{can});$ 
6    $D[\text{the other swap qubit}] \leftarrow D[q_i];$ 
7  $d \leftarrow \text{MAX}(D[\text{swap}.q_0], D[\text{swap}.q_1]) +$ 
8    $\text{SYNTHCOST}(\text{can.MIRROR}()) - \text{SYNTHCOST}(\text{can});$ 
9  $D[\text{swap}.q_0] \leftarrow d; D[\text{swap}.q_1] \leftarrow d;$ 

```

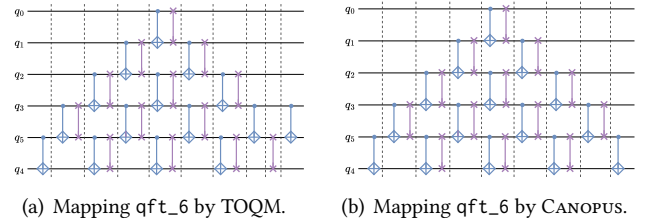


Figure 8. Mapping/routing comparison for the QFT kernel. For convenient visualization, only CPhase and SWAP gates are shown. (a) TOQM generates a sub-optimal mapping scheme, with 2Q depth of 10. (b) CANOPUS generates the optimal scheme in a perfect butterfly structure, with 2Q depth of 9.

Table 1. Qubit routing comparison for the QFT kernel.

QFT kernel		qft_6		qft_12	
Topology	Method	#Can	Depth2Q	#Can	Depth2Q
1D Chain	<i>Optimal</i>	15	9	66	21
	TOQM	16	10	67	22
	CANOPUS	15	9	66	21
2D Square	TOQM	21	13	100	39
	CANOPUS	15	9	75 ($\pm 10\%$)	33 ($\pm 10\%$)

5 Case Studies

We validate the practical advantages of CANOPUS through two realistic case studies: the real-machine compilation and execution of Quantum Fourier Transform (QFT) circuits on IBM’s QPU `ibm_torino`, and the end-to-end simulation of compiled Quantum Low-Density Parity-Check (QLDPC) stabilizer circuits to assess its impact on the logical error rate.

5.1 QFT kernel

QFT is a fundamental subroutine in many promising quantum algorithms, such as Shor’s algorithm [58], quantum phase estimation [32], etc. Given the extensive research on dedicated QFT compilers [30, 42, 69], we select the state-of-the-art compiler TOQM, which specializes in QFT optimization, as our primary baseline.

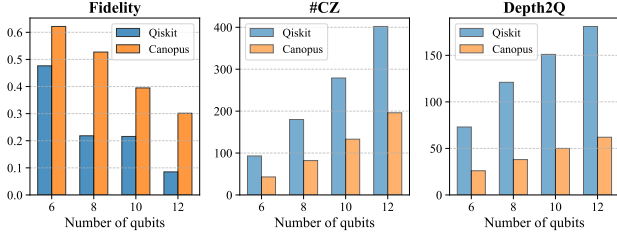


Figure 9. QFT kernel fidelity comparison benchmarked on IBM[®] Quantum Platform (*ibm_torino*). *ibm_torino* is the Heron-series QPU with native gate set $\{CZ, \sqrt{X}, Z(\theta)\}$.

A key finding is that CANOPUS always achieves the optimal QFT routing scheme on the 1D chain topology, while TOQM does not. Provably, the minimal number of SWAP insertions to route an n -qubit QFT is $\frac{n(n-1)}{2} - 2$, that is, 2 fewer than the original CPhase count. This results in a perfect, symmetric butterfly circuit structure, as exemplified in Figure 8(b), with minimal #Can and 2Q circuit depth. Notably, this result is indeed optimal, surpassing the manually designed scheme previously reported as optimal by Maslov [42] where 2 more SWAP gates are required. This optimal scheme is irrespective of the target ISA. In contrast, our experiments show that TOQM despite claiming to realize the scheme from [42], fails to reproduce it and consistently yields inferior results to CANOPUS, as illustrated in Figure 8.

We compare compilation performance for both 6- and 12-qubit QFT kernels on both 1D chain and 2D square topologies, with results summarized in Table 1. On the 1D chain, CANOPUS always produces the theoretically optimal routing result, while TOQM does not. For the small-scale *qft_6* kernel on the 2D square, CANOPUS also achieves the optimal routing, superior to TOQM in both #Can and 2Q depth. For the large-scale *qft_12* kernel, CANOPUS consistently outperforms TOQM in both metrics.

To further validate these results, we performed real-machine experiments on IBM’s *ibm_torino* QPU. We compiled QFT circuits of sizes $n \in \{6, 8, 10, 12\}$ for a 1D chain topology using both CANOPUS and the default QISKIT compiler. Although *ibm_torino* has a heavy-hex topology, it contains linear chains of sufficient size for these benchmarks. Fidelity was measured using the Hellinger fidelity between the experimental and ideal output distributions, with the number of shots set to $\text{MAX}\{4096, 2^n \times 10\}$. A layer of Hadamard gates is appended to each circuit execution so that the ideal final state will be $|0\rangle^{\otimes n}$. In Figure 9, circuits compiled with CANOPUS achieve, on average, a 52.9% reduction in CZ gate count, a 66.4% reduction in 2Q-gate depth, and a 2.1x improvement in fidelity. These results unequivocally demonstrate the practical advantages of CANOPUS for QFT kernel compilation.

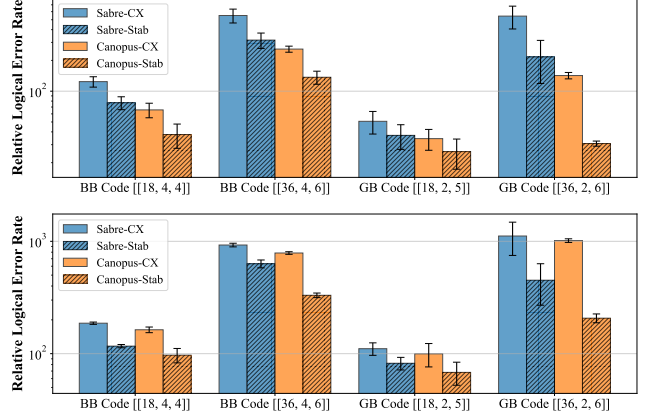


Figure 10. Logical error rate of QLDPC stabilizer circuits compiled for square (top) and heavy-hex (bottom) topologies. The y-axis shows the relative logical error rate normalized by the error rate of an ideal baseline that assumes all-to-all connectivity.

5.2 QLDPC stabilizer circuit

QLDPC codes are rapidly moving from a topic of theoretical interest to a cornerstone of experimental fault-tolerant quantum computing (FTQC) research, mainly because of their superior encoding efficiency [5, 6, 18]. However, due to their frequent long-range interactions [6, 48], realizing QLDPC codes on superconducting processors with fixed, local connectivity is still hampered by significant routing overheads [62].

Therefore, we attempt to compile the circuits automatically under two ISAs: (1) CX ISA with CX as the 2Q basis gate; (2) Stab ISA with both CX and iSWAP as basis gates, assumed to have an identical cost. Particularly, the Stab ISA aligns with practical hardware realities, e.g., both CZ and iSWAP can be natively supported by mainstream superconducting platforms [4, 33, 46, 63]. We further build an end-to-end evaluation pipeline with QLDPC code circuit examples from [48, 62]. We simulate the routed circuits using *stim* [20] under the circuit-level noise model [2, 18]. Finally, all syndromes are decoded using the BPOSD decoder [25, 48, 57] to determine the logical error rate.

As shown in Figure 10, CANOPUS consistently achieves lower logical error rates than SABRE, as the ISA-aware approach of CANOPUS results in compiled circuits with less CX/iSWAP gate count and circuit depth. Under the CX, CANOPUS yields an average logical error suppression of 49.4% on the square topology and 11.4% on the heavy-hex topology compared to SABRE. The advantage becomes even more pronounced with the Stab, where CANOPUS achieves a 52.6% (square) and 29.3% (heavy-hex) error suppression. These results highlight two key findings: first, the ISA-aware mechanism in CANOPUS is highly effective for compiling QEC circuits, and second, the dedicated use of a hybrid CX-iSWAP

Table 2. Selected quantum ISAs.

ISA	2Q basis gates	Description
CX	{CX}	Conventional CX gate
ZZPhase	$\{ZZ_{\frac{\pi}{6}}, ZZ_{\frac{\pi}{4}}, ZZ_{\frac{\pi}{2}}\}$	Discrete CX-family gates, i.e., $\{\sqrt[3]{CX}, \sqrt{CX}, CX\}$ [50]
SQiSW	$\{\sqrt{iSWAP}, iSWAP\}$	Half evolution of iSWAP and iSWAP [26]
ZZPhase_	ZZPhase + $\{pSWAP_{\frac{\pi}{6}, \frac{\pi}{4}, \frac{\pi}{2}}\}$	ZZPhase ISA with the mirror gates
SQiSW_	SQiSW + {ECP, CX}	SQiSW ISA with the mirror gates [45]
Het	ZZPhase + SQiSW	Heterogeneous CX-family and iSWAP-family gates

Table 3. Benchmarks information. These metrics are collected from TKET-optimized logical circuits with only Can and U3 gates. Circuit cost (C_{count} and C_{depth}) is calculated in CX ISA.

Program	#Qubit	#Can	Depth2Q	C_{count}	C_{depth}
bigadder [37]	18	114	79	130.0	88.0
bv [37]	19	18	18	18.0	18.0
ising [37]	26	25	2	50.0	4.0
knn [37]	25	72	50	84.0	62.0
multiplier [37]	15	198	122	222.0	133.0
qec9xz [37]	17	32	12	32.0	12.0
qft [55]	18	153	33	306.0	66.0
qpeexact [55]	16	127	43	260.0	86.0
qram [37]	20	110	70	130.0	78.0
sat [37]	11	210	182	252.0	204.0
swap_test [37]	25	72	50	84.0	62.0
wstate [37]	27	52	28	52.0	28.0

gate set offers a significant practical advantage for QLDPC code demonstrations on superconducting hardware.

6 Evaluation

We further holistically evaluate CANOPUS compared to other leading methods, across representative ISAs and hardware topologies. The evaluation provides both cross-compiler and cross-ISA comparisons under the coherent settings for basis gate cost and routing overhead metric.

6.1 Experimental settings

6.1.1 ISAs and basis gate costs. We consider six different ISAs (including the conventional CX ISA) listed in Table 2. These cover a wide range of powerful basis gates from CX-family and iSWAP-family gates. Particularly, SQiSW [26] proves to a powerful ISA option and has been adopted by recent software projects [22, 45]. ZZPhase ISA containing three fractional $ZZ(\theta)$ rotation gates (equivalently, $\{\sqrt[3]{CX}, \sqrt{CX}, CX\}$) is adopted by QISKIT’s latest synthesis functionalities [28, 50]. For ZZPhase and SQiSW, we also consider the mirror-enhanced version by incorporating the mirrored basis gates [16, 45] into the ISAs. We also include the Het ISA that is the composition of ZZPhase and SQiSW.

To conduct a coherent cross-ISA performance comparison, we use a consistent basis gate cost setting:

$$\left\{ \begin{array}{l} \text{CX} : 1, \text{ZZ}(\pi/t) : 2/t, \sqrt{iSWAP} : 0.75, \\ \text{iSWAP} : 1.5, \text{ECP} : 1.25, \text{pSWAP}(\pi/t) : 2 - 1/t \end{array} \right\}, \quad (4)$$

where CX gate is the unit cost. Such a setting ensures the continuity of gate costs along the critical edges in the Weyl chamber. For example, pSWAP($\pi/2$) is equivalent to iSWAP and they have the same cost of 1.5. With a specific gate family, basis gates with larger canonical coefficients usually requires proportionally longer interaction time on physical qubits, which was reflected in the cost setting. Note that this setting is a comprehensive consideration for current gate schemes and hardware-implemented gate fidelities in superconducting [1, 4, 12, 46, 63]. It is neither limited to a specific gate scheme nor a specific hardware platform.

6.1.2 Metrics. With the consistent basis gate cost settings above, we can evaluate cross-ISA circuit cost comparison, in terms of both gate count (C_{count}) and circuit depth (C_{depth}). Specifically, C_{count} refers to the sum of all 2Q gate costs according to the basis gate setting in Equation (4). C_{depth} refers to the length of the cost-weighted critical path within the circuit DAG. C_{count} and C_{depth} are naturally the generalized metrics for 2Q gate count and circuit depth. To quantify the routing effects across ISAs and topologies, we define the routing overhead as the ratio of routed circuit cost to the pre-routed circuit cost, for which the pre-routed logical-level circuit cost is uniformly computed in the CX ISA.

6.1.3 Benchmarks. We select a set of medium-size benchmarks from QASMBench [37] and MQTBench [55] spanning various categories of quantum programs. These benchmarks first go through logical-level optimization by TKET and are rebased to {Can, U3} as the input of the evaluated compilers. Information for benchmarks after logical optimization is summarized in Table 3.

6.1.4 Baselines. The leading methods SABRE, TOQM, and BQSKIT are selected as the baselines. Both SABRE and CANOPUS are implemented in the Python-based QISKIT framework, i.e., we do not use the Rust-accelerated SABRE implementation in the latest QISKIT version, for fair runtime comparison. TOQM is the SOTA circuit depth driven qubit routing method [69]. We also select BQSKIT as a baseline as it represents another different cross-ISA compilation paradigm [67]. Given a target gate set and coupling graph, BQSKIT performs end-to-end compilation via numerical optimization, that is, finally the rebased circuit is generated.

Hyperparameters for SABRE and CANOPUS are of the same settings. Each performs 10 times layout procedure, within which 5-round bidirectional passes are proceeded and each pass performs 10 trials. The best result across all attempts is selected. TOQM can obtain the deterministic routing result in one go. Compiled circuits by BQSKIT, although in terms

Table 4. Average (geometric-mean) routing overhead across different topologies and backend ISAs.

Routing overhead		In terms of C_{count}				In terms of C_{depth}			
Topo	ISA Type	<i>sabre</i>	<i>toqm</i>	<i>bqskit</i>	<i>canop</i>	<i>sabre</i>	<i>toqm</i>	<i>bqskit</i>	<i>canop</i>
Chain	CX	2.26	3.07	2.27	1.88	2.57	2.38	2.18	1.81
	ZZPhase	1.97	2.75	1.92	1.7	2.22	2.15	1.91	1.63
	SQiSW	2.06	2.63	1.85	1.73	2.32	2.08	1.84	1.68
	ZZPhase_	1.61	2.18	1.69	1.39	1.82	1.72	1.66	1.35
	SQiSW_	1.72	2.25	1.68	1.45	1.95	1.76	1.66	1.4
	Het	1.65	2.23	1.58	1.43	1.86	1.76	1.56	1.36
HHex	CX	2.37	2.82	2.59	1.93	3.05	2.68	2.66	2.08
	ZZPhase	2.12	2.65	2.25	1.74	2.77	2.52	2.26	1.91
	SQiSW	2.14	2.48	2.17	1.72	2.71	2.43	2.28	1.96
	ZZPhase_	1.7	2.08	1.88	1.4	2.2	2.0	1.96	1.56
	SQiSW_	1.78	2.09	1.98	1.46	2.27	2.02	2.1	1.66
	Het	1.74	2.13	1.86	1.43	2.25	2.05	1.98	1.58
Square	CX	1.64	2.18	2.06	1.38	1.94	1.87	2.47	1.49
	ZZPhase	1.35	1.87	1.61	1.16	1.63	1.61	1.94	1.24
	SQiSW	1.63	2.05	1.74	1.34	1.89	1.81	2.02	1.42
	ZZPhase_	1.16	1.55	1.43	0.99	1.39	1.36	1.65	1.09
	SQiSW_	1.31	1.69	1.56	1.11	1.54	1.47	1.83	1.2
	Het	1.18	1.58	1.36	1.0	1.41	1.38	1.56	1.09

of only the 2Q gates, is also random. Thus we perform 3 trials for each input case and report the best result.

6.2 Suppression of routing overhead

The comprehensive evaluation (on geometric-mean average) results are summarized in Table 4, across the six selected ISAs and three hardware topologies (1D chain, 2D heavy-hex, 2D square). While detailed results across the $3 \times 6 \times 12$ cases are listed in Table 5 and Table 6 in Appendix C. CANOPUS results in the lowest average (geometric-mean) routing overhead for each ISA-topology combination benchmarking, significantly surpassing other methods. Specifically, the routing overhead reduction achieved by CANOPUS is on average 16.06% (26.44%), 34.70% (21.25%), and 19.89% (20.72%) in terms of C_{count} (C_{depth}), compared to SABRE, TOQM, and BQSKIT, respectively. With CANOPUS, those more powerful ISAs, such as ZZPhase and SQiSW ISAs, actually exhibit significantly lower routing overhead than CX. While the baseline methods do not apparently indicate that, for which the circuit cost reduction stems from ISA rebase itself.

Notably, SABRE and BQSKIT focus on gate count driven optimization, TOQM specializes in lowering circuit depth, while our CANOPUS involves both count and depth related optimization. Among them, TOQM leads to the worst count-related routing overhead. Even for the routing overhead in terms of depth, TOQM consistently underperforms CANOPUS, and it only outperforms BQSKIT for 2D square topology. Besides, CANOPUS could manage the routing overhead in a ubiquitously low level, in terms of both count and depth costs; while every baseline fails to optimize some specific circuits. For example, TOQM/BQSKIT cannot manage the

routing overhead for qec9 circuit; BQSKIT cannot for bv circuit, even though with more expressive ISAs.

6.3 Program-ISA-Topology co-exploration

Our evaluation also systematically explores how program patterns, ISA selection, and hardware topologies impact each other. We highlight some guidelines for optimal co-design particularly according to results achieved by CANOPUS (Table 4, Table 5, Table 6): ① Heavy-hex topology consistently leads to higher routing overhead across all these ISAs, compared to the seemingly more sparse 1D chain topology. This is mostly because most quantum algorithms are constructed in a subroutine-unrolling approach, naturally more friendly with chain topology. The QFT kernel detailed in Section 5.1 is a thorough good example. ② The combinatorial ISA involving both CX-family and iSWAP-family gates is much superior to either sole one. Specifically, either ZZPhase or SQiSW could lead to no more than 11% routing overhead reduction compared to CX, while Het results in more than 25% reduction than CX. This benefit is more significant for circuits largely containing CX/CZ as 2Q blocks such as qec9. ③ Gate mirroring is another approach to designing powerful quantum ISAs, as both ZZPhase and SQiSW achieve comparable results to Het ISA. This is due to the same optimization opportunities brought by SWAP mirroring. ④ For Hamiltonian simulation programs like *ising*, ZZPhase is essential to improve execution performance. Therein multiple 2-local Pauli rotations equivalent to $XX(\theta)$ are included. As a discrete fractional $XX(\theta)$ basis gate set, ZZPhase ISA is more suitable than other gate family selections in this case.

The real-machine experiment in Section 5.1 showcases how our method can help achieve superior compilation results and thus higher program fidelities for QFT kernels using the standard CX ISA (CZ on *ibm_torino*). However, extending this real-machine validation to alternative ISAs is currently challenging due to the scarcity of quantum processors equipped with well-calibrated heterogeneous gate sets. For instance, while IBM has proposed fractional gates, i.e., the continuous $ZZ(\theta)$ gate set [27], their implementation details and calibration procedures are not publicly disclosed. To our knowledge, the $ZZ(\theta)$ gates have the same duration as CZ on IBM’s Heron QPUs regardless of the rotation angle, and their error rates are consistently 1x-3x that of CZ. This performance is far from the ideal assumptions of ZZPhase. Fortunately, a path forward is emerging with the recently proposed AshN gate scheme [11] that enables directly implementing any basis gates with the optimal gate durations. It is also experimentally evinced on transmon qubits by Chen et al. [12], where multiple basis gates are calibrated in high fidelities that aligns with our cost model as well. This development may enable comprehensive, real-machine co-exploration of programs, ISAs, and hardware topologies in the near future.

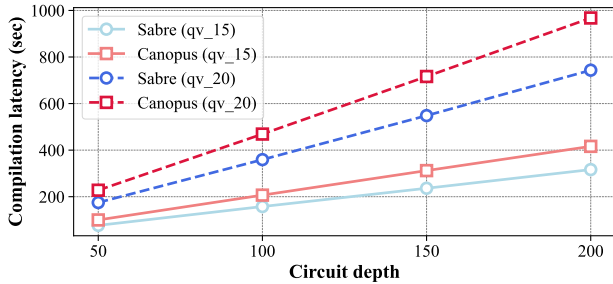


Figure 11. Compilation latency comparison.

6.4 Diverse-ISA compilation paradigms

Prior to this work, there are two major compilation paradigms targeting diverse ISAs: (1) Use the conventional compiler that operates entirely on the CX-based circuit representation before ISA rebase. The final-stage rebase pass can usually be completed via optimal synthesis in efficient analytical or numerical computation [26, 44, 50, 61]. (2) Use brute-force approximate synthesis to perform structural search and numerical optimization to determine the synthesized circuit with minimal gate count [17, 34, 49]. SABRE/TOQM and BQSKIT are representative of these two paradigms, respectively. In our evaluation, BQSKIT even underperforms the industrial-standard SABRE in most cases. Exceptionally, in terms of the circuit depth, BQSKIT leads to better results than other baselines on sparse topologies (chain, heavy-hex), as its A^* -based search for 2Q gate arrangement could exhibit advantages over long-range qubit routing, but this advantage does not hold for more connected topologies. Besides, the second numerical optimization based paradigm is of exponential computational complexity. For benchmarking the 216 medium-size cases in Table 5, the Rust-backend BQSKIT requires on average 18 minutes to process each circuit with an Apple M3 Max CPU; in contrast, the Python-implemented SABRE requires only 17 seconds. Consequently, this second paradigm is ill-suited for compiling real-world programs, proving both ineffective and inefficient when targeting diverse ISAs (at least for discrete gate sets). Instead, although there is a gap between the conventional routing model and backend ISA properties, by means of routing-synthesis co-optimization, the first paradigm could be enhanced to bridge the gap between the routing model and backend ISA properties and thus provides a more viable path.

6.5 Runtime analysis

In our field tests for the set of benchmarks above, CANOPUS consistently exhibits 1x-2x runtime latency of SABRE. This result aligns with the complexity analysis in Section 4.5. Herein we specifically demonstrate the end-to-end runtime analysis for larger-scale quantum circuits. We use random

quantum volume [16] circuits generated by QISKIT for scalability benchmarking, which represent the most complicated circuit structures with dense 2Q gate arrangement. Each canonical gate within the quantum volume circuit contains unique canonical parameters as each 2Q unitary is randomly generated, thus there is no cached synthesis cost calculation for performance improvement in one pass. We select quantum volume circuits with two different widths (number of qubits), 15 and 20. We vary the depth of these circuits (qv_15 and qv_20) from 50 to 200. The largest size of these qv circuits is up to thousands of 2Q gates. As Figure 11 shows, CANOPUS leads to an average 1.31x ($\pm 1\%$) latency compared to SABRE for each benchmarked circuit. Both compilers’ latency scales linearly with circuit depth and width. If we compare the curve slopes, CANOPUS leads to 1.32x (1.30x) latency scaling slope compared to that of SABRE in terms of depth for qv_15 (qv_20) circuits.

7 Related Work

Qubit mapping/routing is one of the most well-explored topics of quantum compiler research, as it shares similar methodologies with instruction scheduling [14, 24] and register allocation [9, 52] in classical computing.

To perform scalable qubit routing, Zulehner et al. [73] introduces an A^* -based algorithm to minimize SWAP gate overhead for concurrent CX gate layers. The approach partitions the circuit into layers and solves the mapping problem subsequently. Li et al. [38] also utilizes the circuit DAG layering thought and proposes a bidirectional routing procedure SABRE to find better initial mappings thus with lower SWAP insertion count. It also briefly discusses the trade-off between the inserted SWAP count and the circuit depth but does not prioritize optimizing circuit depth. Subsequent works have aimed to improve circuit depth and parallelism, either by using SABRE-like heuristics [3, 35, 72] or graph matching techniques [13]. Zhang et al. [69] systematically investigates the depth-optimality of qubit mapping and proposes an A^* -based method TOQM that reported superior performance over existing solver-based depth-driven approaches [59]. However, holistic optimality of qubit routing is contingent on the specific ISA, device topology, and circuit cost model, and is rarely guaranteed by theoretical bounds. Indeed, our own evaluation reveals that TOQM does not always produce depth-optimal results compared to our heuristic, CANOPUS. For example, our case study in Section 5.1 demonstrates that the mapping scheme for the QFT kernel, purported to be optimal in their analysis, can be further improved.

With the recent development of advanced quantum ISAs such as superconducting fractional gates [27], ion-trapped partial entangling gates [29, 65], and the AshN gates [11, 12], some works have begun exploring how to efficiently utilize these ISAs to make compiler optimizations closer to hardware characteristics. McKinney et al. [45] investigates the

practical performance of `QISWISA` proposed by Huang et al. [26] and the synthesis capability when incorporating the basis gates' mirrors into the ISA. Their modified `SABRE` algorithm offers a preliminary attempt at the collaborative gate decomposition and qubit routing approach, while the optimization opportunities considered therein are limited and the algorithmic techniques are not sophisticated. `BQSKIT` [67] and the series of works behind it [17, 34, 64, 68] provide a toolkit to rebase arbitrary 2Q unitaries to specific ISAs through approximate synthesis (structural search and numerical optimization) which is not computationally efficient. Approximate synthesis by `BQSKIT` does not ensure optimal schemes for two-qubit and multi-qubit circuit synthesis. In addition, due to the lack of native compilation strategies and a rational synthesis cost model, Kalloor et al. [31] claims that alternative ISAs are hardly comparable to `CX` when evaluating quantum hardware roofline by `BQSKIT`. As for applicability of expanded ISAs to QEC, Google's latest theoretical [43] and experimental [19] works demonstrate the `CX-iSWAP` combination ISA could help suppress the fault-tolerant threshold. Zhou et al. [71] proposes a routing-based method enhanced by `CX-iSWAP` for overcoming ancilla defects among surface code blocks while preserving encoded logical information, but it relies on manual design and experience.

8 Conclusion

In our work, we introduce `CANOPUS`, the first unified, ISA-aware qubit routing framework designed to operate across diverse quantum hardware. By leveraging a canonical two-qubit gate representation and a formal cost model derived from monodromy polytope theory, `CANOPUS` achieves deep co-optimization of qubit routing and gate synthesis. This approach not only demonstrates the practical superiority of emerging quantum ISAs but also enables systematic co-exploration of how different ISAs, program patterns, and hardware topologies interact, providing a powerful new tool for quantum system design.

References

- [1] Rajeev Acharya, Dmitry A. Abanin, Laleh Aghababaie-Beni, Igor Aleiner, Trond I. Andersen, Markus Ansmann, Frank Arute, Kunal Arya, Abraham Asfaw, Nikita Astrakhantsev, Juan Atalaya, Ryan Babbush, Dave Bacon, Brian Ballard, Joseph C. Bardin, Johannes Bausch, Andreas Bengtsson, Alexander Bilmes, Sam Blackwell, Sergio Boixo, Gina Bortoli, Alexander Boussass, Jenna Bovaird, Leon Brill, Michael Broughton, David A. Browne, Brett Buchea, Bob B. Buckley, David A. Buell, Tim Burger, Brian Burkett, Nicholas Bushnell, Anthony Cabrera, Juan Campero, Hung-Sheng Chang, Yu Chen, Zijun Chen, Ben Chiaro, Desmond Chik, Charina Chou, Jan Claes, Amenta Y. Clam-baneanu, Josh Cong, Roberto Collins, Paul Conner, William Courmier, Alexander L. Crook, Ben Curtin, Sayan Das, Alex Davies, Laura De Lorezzo, Dristo M. Debry, Sean Denver, Michael Devoret, Augustin Di Paolo, Paul Donoho, Illy Drozdov, Andrew Dunsworth, Clint Eark, Thanes Elich, Alec Eickbusch, Aviv Moshe Elbag, Mahmoud Elzouka, Catherine Erickson, Lara Faoro, Edward Farhi, Vincicus S. Ferreira, Leslie Fores Burgos, Ebrahim Forati, Austin G. Fowler, Brooks Foxen,
- Subas Ganjam, Gonzalo Garcia, Robert Gasca, Elie Genois, William Giang, Craig Gidney, Dar Gilboa, Rajan Gokhale, Alejandro Grajales Daul, Dietrich Grauman, Alex Greene, Jonathan A. Gross, Steve Habegger, John Hall, Michael C. Hamilton, Monica Hansen, Matthew Harrigan, Sean D. Harrington, Francisco J.H. Heras, Stephen Hincks, Paula Hoel, Oscar Higgott, Gordon Hill, Jeremy Hilton, George Holland, Sabrina Hong, Hsin-Yuan Huang, Ashley Huff, William J. Huggins, Lev B. Ioffe, Sergei V. Isakov, J. Justin Iveland, Evan Jeffrey, Zhang Jiang, Cody Jones, Stephen Jordan, Chitartil John, Pavol Juhás, Dvir Kafri, Hui Kang, Amir H. Karamlou, Kostantyn Kechedzhi, Julian Kelly, Trupt Khaire, Tanuj H. Khattar, Seon Kim, Paul V. Klimov, Andrey R. Klots, Bryce Kobrin, Pushmeet Kohli, Alexander N. Korotkov, Fedor Kostritsa, Robin Kothari, Borislav Kozlovskii, John Mark Kreikebaum, Vladislav D. Kurilovich, Nathan Lacroix, David Landhuis, Tiano Lange-Dei, Brandon W. Langley, Pavel Laptev, Kim-Ming Lau, Loick Le Guevel, Justin Ledford, Joonho Lee, Kennley Lee, Yuri D. Lensky, Shannon Leon, Brian J. Lester, Wing Yan Li, Yin Li, Alexander T. Lili, Wayee Liu, William P. Livingston, Aditya Locharla, Erik Lucero, Daniel Lundahl, Aaron Luni, Sid Madhuk, Finnon D. Malone, Ashley Maloney, Salvatore Mandra, James Manyika, Leigh S. Martin, Orion Martin, Steven Martin, Cameron Marfield, Jarrod R. McClean, Matt McEwen, Seneca Meeks, Anthony Megrant, Xiao Mi, Kevin C. Miao, Amanda Mieszala, Reza Mola, Sebastian Molina, Shirin Montazeri, Alexis Morvan, Ramis Moussa, Wojciech Muczkiwicz, Ofer Naaman, Matthew Neeley, Charles Neil, Ani Nersisyan, Hartmut Neven, Michael Newman, Jun How Ng, Anthony Nguyen, Murray Nguyen, Chia-Hung Ni, Murphy Yuezhen Niu, Thomas E. O'Brien, William D. Oliver, Alex Opremcak, Kristoffer Ottosson, Andre Petukhov, Alex Pizzito, John Platt, Rebecca Potter, Orion Pritchard, Leonid P. Pryadko, Chris Quintana, Ganesh Ramachandran, Matthew J. Reagor, John Redding, Dadi M. Rados, Gabrielle Roberts, Elliott Rosenberg, Emma Rosenfeld, Pedram Roushan, Nicholas C. Rubin, New Year Saei, Daniel Sank, Kannan Sankaragomathi, Kevin J. Satzinger, Henry F. Schurkus, Christopher Shuster, Andrew W. Senior, Michael J. Shearn, Aaron Shorter, Noah Shetty, Vladimir Shvarts, Shradha Singh, Volodymyr Sivak, Jindra Skrzyny, Spencer Small, Vadim Smelyanskiy, W. Clarke Smith, Rolando Somma, Sofia Springer, George Sterling, Doug Strain, Jordan Suchard, Aaron Szasz, Alex Szein, Douglas Thor, Alfredo Torres, M. Mert Torubaldi, Abeer Vishnav, Justin Vargas, Sergey Vdovichev, Guifre Vidal, Benjamin Villalonga, Catherine Vollgraff Heidweiller, Steven Waltman, Shannon X. Wang, Brayden Ware, Kate Weber, Travis Weidel, Theodore White, Kristi Wong, Bryan W.K. Woo, Cheng Xing, Z. Jamie Yao, Ping Yeh, Bicheng Ying, Juhwan Yoo, Nourelin Yost, Grayson Young, Adam Zalcman, Yaxing Zhang, Ningfeng Zhu, and Nicholas Zobrist. 2024. Quantum error correction below the surface code threshold. *Nature* 638, 8052 (2024), 920.
- [2] Rajeev Acharya, I. Aleiner, Richard Allen, Trond I. Andersen, Markus Ansmann, Frank Arute, Kunal Arya, Abraham T. Asfaw, Juan Atalaya, Ryan Babbush, Dave Bacon, Joseph C. Bardin, João Marcos Vensi Basso, Andreas Bengtsson, Sergio Boixo, Gina Bortoli, Alexandre Bourassa, Jenna Bovaird, Leon Brill, Mick Broughton, Bob B. Buckley, David A. Buell, Tim Burger, Brian Burkett, Nicholas Bushnell, Yu Chen, Zijun Chen, Benjamin Chiaro, J. Zachery Cogan, Roberto Collins, P. N. Conner, William Courtney, Alexander L. Crook, B Curtin, Dripto M. Debroy, A Del Toro Barba, Sean Demura, Andrew Dunsworth, Daniel Eppens, Catherine Erickson, Lara Faoro, Edward Farhi, Reza Fatemi, Leslie Flores Burgos, Ebrahim Forati, Austin G. Fowler, Brooks Foxen, William Giang, Craig Gidney, Dar Gilboa, Marissa Giustina, Alejandro Grajales Dau, Jonathan A. Gross, S. Habegger, Michael C. Hamilton, Matthew P. Harrigan, Sean D. Harrington, Oscar Higgott, Jeremy P. Hilton, Michael J. Hoffmann, Sabrina Hong, Trent Huang, Ashley Huff, William J. Huggins, L. B. Ioffe, Sergei V. Isakov, Justin Iveland, Evan Jeffrey, Zhang Jiang, Cody Jones, Pavol Juhás, Dvir Kafri, Kostyantyn Kechedzhi, Julian Kelly, Tanuj Khattar, Mostafa Khezri,

- M'aria Kieferov'a, Seon Kim, Alexei Kitaev, Paul V. Klimov, Andrey R. Klots, Alexander N. Korotkov, Fedor Kostritsa, John Mark Kreikebaum, David Landhuis, Pavel Laptev, Kim Ming Lau, Lily Laws, Joonho Lee, Kenny Lee, Brian J. Lester, Alexander T Lill, Wayne Liu, Aditya Locharla, Erik Lucero, Fionn D. Malone, Jeffrey Marshall, Orion Martin, Jarrod R. McClean, Trevor McCourt, Matthew J. McEwen, Anthony Megrant, Bernardo Meurer Costa, Xiao Mi, Kevin C. Miao, Masoud Mohseni, Shirin Montazeri, Alexis Morvan, Emily Mount, Wojciech Mruzekiewicz, Ofer Naaman, Matthew Neeley, Charles J. Neill, Ani Nersisyan, Hartmut Neven, Michael Newman, Jiun How Ng, Anthony Nguyen, Murray L. Nguyen, Murphy Yuezhen Niu, Thomas E. O'Brien, Alexander Opremcak, J. Platt, Andre Petukhov, Rebecca Potter, Leonid P. Pryadko, Chris Quintana, Pedram Roushan, Nicholas C. Rubin, Negar Saei, Daniel Thomas Sank, K Sankaragomathi, Kevin J. Satzinger, Henry F. Schurkus, C. Schuster, Michael Shearn, Aaron Shorter, Vladimir Shvarts, Jindra Skruzny, Vadim N. Smelyanskiy, William C. Smith, George Sterling, Doug Strain, Yuan Su, Marco Szalay, Alfredo Torres, Guifre Vidal, Benjamin Villalonga, Catherine Vollgraff Heidweiler, Theodore White, Chen Xing, Z. Jamie Yao, Ping Yeh, Juhwan Yoo, Grayson Young, Adam Zalcman, Yaxing Zhang, and Ningfeng Zhu. 2022. Suppressing quantum errors by scaling a surface code logical qubit. *Nature* 614 (2022), 676 – 681.
- [3] Alessandro Annechini, Marco Venere, Donatella Sciuto, and Marco Santambrogio. 2025. DDRoute: a Novel Depth-Driven Approach to the Qubit Routing Problem. In *Proceedings of the 62st ACM/IEEE Design Automation Conference*.
- [4] Frank Arute, Kunal Arya, Ryan Babbush, Dave Bacon, Joseph C. Bardin, Rami Barends, Rupak Biswas, Sergio Boixo, Fernando G. S. L. Brandao, David A. Buell, Brian Burkett, Yu Chen, Zijun Chen, Ben Chiaro, Roberto Collins, William Courtney, Andrew Dunsworth, Edward Farhi, Brooks Foxen, Austin Fowler, Craig Gidney, Marissa Giustina, Rob Graff, Keith Guerin, Steve Habegger, Matthew P. Harrigan, Michael J. Hartmann, Alan Ho, Markus Hoffmann, Trent Huang, Travis S. Humble, Sergei V. Isakov, Evan Jeffrey, Zhang Jiang, Dvir Kafri, Kostyantyn Kechedzhi, Julian Kelly, Paul V. Klimov, Sergey Knysh, Alexander Korotkov, Fedor Kostritsa, David Landhuis, Mike Lindmark, Erik Lucero, Dmitry Lyakh, Salvatore Mandrà, Jarrod R. McClean, Matthew McEwen, Anthony Megrant, Xiao Mi, Kristel Michielsen, Masoud Mohseni, Josh Mutus, Ofer Naaman, Matthew Neeley, Charles Neill, Murphy Yuezhen Niu, Eric Ostby, Andre Petukhov, John C. Platt, Chris Quintana, Eleanor G. Rieffel, Pedram Roushan, Nicholas C. Rubin, Daniel Sank, Kevin J. Satzinger, Vadim Smelyanskiy, Kevin J. Sung, Matthew D. Trevithick, Amit Vainsencher, Benjamin Villalonga, Theodore White, Z. Jamie Yao, Ping Yeh, Adam Zalcman, Hartmut Neven, and John M. Martinis. 2019. Quantum supremacy using a programmable superconducting processor. *Nature* 574, 7779 (2019), 505–510.
- [5] Sergey Bravyi, Andrew W Cross, Jay M Gambetta, Dmitri Maslov, Patrick Rall, and Theodore J Yoder. 2024. High-threshold and low-overhead fault-tolerant quantum memory. *Nature* 627, 8005 (2024), 778–782.
- [6] Nikolas P Breuckmann and Jens Niklas Eberhardt. 2021. Quantum low-density parity-check codes. *PRX Quantum* 2, 4 (2021), 040101.
- [7] Colin D Bruzewicz, John Chiaverini, Robert McConnell, and Jeremy M Sage. 2019. Trapped-ion quantum computing: Progress and challenges. *Applied Physics Reviews* 6, 2 (2019), 021314.
- [8] Stephen S Bullock and Igor L Markov. 2003. An arbitrary two-qubit computation in 23 elementary gates or less. In *Proceedings of the 40th Annual Design Automation Conference*. IEEE, Anaheim, CA, USA, 324–329.
- [9] Gregory J Chaitin. 1982. Register allocation & spilling via graph coloring. *ACM Sigplan Notices* 17, 6 (1982), 98–101.
- [10] Christopher Chamberland, Guanyu Zhu, Theodore J Yoder, Jared B Hertzberg, and Andrew W Cross. 2020. Topological and subsystem codes on low-degree graphs with flag qubits. *Physical Review X* 10, 1 (2020), 011022.
- [11] Jianxin Chen, Dawei Ding, Weiyuan Gong, Cupjin Huang, and Qi Ye. 2024. One Gate Scheme to Rule Them All: Introducing a Complex Yet Reduced Instruction Set for Quantum Computing. In *Proceedings of the 29th ACM International Conference on Architectural Support for Programming Languages and Operating Systems, Volume 2*. ACM, La Jolla, CA, USA, 779–796.
- [12] Zhen Chen, Weiyang Liu, Yanjun Ma, Weijie Sun, Ruixia Wang, He Wang, Huikai Xu, Guangming Xue, Haisheng Yan, Zhen Yang, Jiayu Ding, Yang Gao, Feiyu Li, Yujia Zhang, Zikang Zhang, Yirong Jin, Haifeng Yu, Jianxin Chen, and Fei Yan. 2025. Efficient implementation of arbitrary two-qubit gates using unified control. *Nature Physics* (15 Aug 2025). doi:10.1038/s41567-025-02990-x
- [13] Andrew M Childs, Eddie Schoute, and Cem M Unsal. 2019. Circuit transformations for quantum architectures. *arXiv preprint arXiv:1902.09102* (2019).
- [14] Josep M Codina, Jesús Sánchez, and Antonio González. 2001. A unified modulo scheduling and register allocation technique for clustered processors. In *Proceedings 2001 International Conference on Parallel Architectures and Compilation Techniques*. IEEE, 175–184.
- [15] Gavin E Crooks. 2020. Gates, states, and circuits. Available at <https://threeplusone.com/pubs/on-gates-v0-5/>.
- [16] Andrew W Cross, Lev S Bishop, Sarah Sheldon, Paul D Nation, and Jay M Gambetta. 2019. Validating quantum computers using randomized model circuits. *Physical Review A* 100, 3 (2019), 032328.
- [17] Marc Grau Davis, Ethan Smith, Ana Tudor, Koushik Sen, Irfan Siddiqi, and Costin Iancu. 2019. Heuristics for quantum compiling with a continuous gate set. 12 pages. arXiv preprint arXiv:1912.02727.
- [18] Eric Dennis, Alexei Kitaev, Andrew Landahl, and John Preskill. 2002. Topological quantum memory. *J. Math. Phys.* 43, 9 (2002), 4452–4505.
- [19] Alec Eickbusch, Matt McEwen, Volodymyr Sivak, Alexandre Bourassa, Juan Atalaya, Jahan Claes, Dvir Kafri, Craig Gidney, Christopher W. Warren, Jonathan Gross, Alex Opremcak, Nicholas Zobrist, Kevin C. Miao, Gabrielle Roberts, Kevin J. Satzinger, Andreas Bengtsson, Matthew Neeley, William P. Livingston, Alex Greene, Rajeev Acharya, Laleh Aghababaie Beni, Georg Aigeldinger, Ross Alcaraz, Trond I. Andersen, Markus Ansmann, Frank Arute, Kunal Arya, Abraham Asfaw, Ryan Babbush, Brian Ballard, Joseph C. Bardin, Alexander Balmes, Jenna Bovaird, Dylan Bowers, Leon Brill, Michael Broughton, David A. Browne, Brett Buchea, Bob B. Buckley, Tim Burger, Brian Burkett, Nicholas Bushnell, Anthony Cabrera, Juan Campero, Hung-Shen Chang, Ben Chiaro, Liang-Ying Chih, Agnetta Y. Cleland, Josh Cogan, Roberto Collins, Paul Conner, William Courtney, Alexander L. Crook, Ben Curtin, Sayan Das, Alexander Del Toro Barba, Sean Demura, Laura De Lorenzo, Agustin Di Paolo, Paul Donohoe, Ilya K. Drozdov, Andrew Dunsworth, Aviv Moshe Elbag, Mahmoud Elzouka, Catherine Erickson, Vinicius S. Ferreira, Leslie Flores Burgos, Ebrahim Forati, Austin G. Fowler, Brooks Foxen, Suhas Ganjam, Gonzalo Garcia, Robert Gasca, Élie Genois, William Giang, Dar Gilboa, Raja Gosula, Alejandro Grajales Dau, Dietrich Graumann, Tan Ha, Steve Habegger, Monica Hansen, Matthew P. Harrigan, Sean D. Harrington, Stephen Heslin, Paula Heu, Oscar Higgott, Reno Hiltermann, Jeremy Hilton, Hsin-Yuan Huang, Ashley Huff, William J. Huggins, Evan Jeffrey, Zhang Jiang, Xiaoxuan Jin, Cody Jones, Chaitali Joshi, Pavol Juhas, Andreas Kabel, Hui Kang, Amir H. Karamlou, Kostyantyn Kechedzhi, Trupti Khaire, Tanuj Khattar, Mostafa Khezri, Seon Kim, Bryce Kobrin, Alexander N. Korotkov, Fedor Kostritsa, John Mark Kreikebaum, Vladislav D. Kurilovich, David Landhuis, Tiano Lange-Dei, Brandon W. Langley, Kim-Ming Lau, Justin Ledford, Kenny Lee, Brian J. Lester, Loïck Le Guevel, Wing Yan Li, Alexander T. Lill, Aditya Locharla, Erik Lucero, Daniel Lundahl, Aaron Lunt, Sid Madhuk, Ashley Maloney, Salvatore Mandrà, Leigh S. Martin, Orion Martin, Cameron Maxfield, Jarrod R. McClean, Seneca Meeks, Anthony Megrant, Reza Molavi,

- Sebastian Molina, Shirin Montazeri, Ramis Movassagh, Michael Newman, Anthony Nguyen, Murray Nguyen, Chia-Hung Ni, Logan Oas, Raymond Orosco, Kristoffer Ottosson, Alex Pizzuto, Rebecca Potter, Orion Pritchard, Chris Quintana, Ganesh Ramachandran, Matthew J. Reagor, David M. Rhodes, Elliott Rosenberg, Elizabeth Rossi, Kannan Sankaragomathi, Henry F. Schurkus, Michael J. Shearn, Aaron Shorter, Noah Shutty, Vladimir Shvarts, Spencer Small, W. Clarke Smith, Sofia Springer, George Sterling, Jordan Suchard, Aaron Szasz, Alex Sztejn, Douglas Thor, Eifu Tomita, Alfredo Torres, M. Mert Torunbalci, Abeer Vaishnav, Justin Vargas, Sergey Vdovichev, Guifre Vidal, Catherine Vollgraff Heidweiller, Steven Waltman, Jonathan Waltz, Shannon X. Wang, Brayden Ware, Travis Weidel, Theodore White, Kristi Wong, Bryan W. K. Woo, Maddy Woodson, Cheng Xing, Z. Jamie Yao, Ping Yeh, Bicheng Ying, Juhwan Yoo, Noureldin Yosri, Grayson Young, Adam Zalzman, Yaxing Zhang, Ningfeng Zhu, Sergio Boixo, Julian Kelly, Vadim Smelyanskiy, Hartmut Neven, Dave Bacon, Zijun Chen, Paul V. Klimov, Pedram Roushan, Charles Neill, Yu Chen, and Alexis Morvan. 2024. Demonstrating dynamic surface codes. *arXiv preprint arXiv:2412.14360* (2024).
- [20] Craig Gidney. 2021. Stim: a fast stabilizer circuit simulator. *Quantum* 5 (2021), 497. <https://api.semanticscholar.org/CorpusID:232104816>
- [21] Michael Goerz and Evan McKinney. 2024. weylchamber: Python package for analyzing two-qubit gates in the Weyl chamber. <https://pypi.org/project/weylchamber/>. Python package.
- [22] Google Quantum AI. 2025. Cirq API. https://quantumai.google/reference/python/cirq/two_qubit_matrix_to_sqrt_iswap_operations.
- [23] Aram W Harrow, Avinatan Hassidim, and Seth Lloyd. 2009. Quantum algorithm for linear systems of equations. *Physical review letters* 103, 15 (2009), 150502.
- [24] John L Hennessy and Thomas Gross. 1983. Postpass code optimization of pipeline constraints. *ACM Transactions on Programming Languages and Systems (TOPLAS)* 5, 3 (1983), 422–448.
- [25] Timo Hillmann, Lucas Berent, Armanda O Quintavalle, Jens Eisert, Robert Wille, and Joschka Roffe. 2024. Localized statistics decoding: A parallel decoding algorithm for quantum low-density parity-check codes. *arXiv preprint arXiv:2406.18655* (2024).
- [26] Cupjin Huang, Tenghui Wang, Feng Wu, Dawei Ding, Qi Ye, Linghang Kong, Fang Zhang, Xiaotong Ni, Zhijun Song, Yaoyun Shi, Hui-Hai Zhao, Chunqing Deng, and Jianxin Chen. 2023. Quantum Instruction Set Design for Performance. *Physical Review Letters* 130 (Feb 2023), 070601. Issue 7. doi:10.1103/PhysRevLett.130.070601
- [27] IBM Quantum. 2024. New fractional gates reduce circuit depth for utility-scale workloads. <https://www.ibm.com/quantum/blog/fractional-gates>. Accessed: Nov. 18, 2024.
- [28] IBM Quantum. 2025. Qiskit API. <https://quantum.cloud.ibm.com/docs/en/api/qiskit/qiskit.synthesis.XXDecomposer>.
- [29] IonQ. 2023. Getting started with IonQ’s hardware-native gateset. <https://docs.ionq.com/guides/getting-started-with-native-gates>.
- [30] Yuwei Jin, Xiangyu Gao, Minghao Guo, Henry Chen, Fei Hua, Chi Zhang, and Eddy Z Zhang. 2024. Optimizing quantum fourier transformation (qft) kernels for modern nisq and ft architectures. In *SC24: International Conference for High Performance Computing, Networking, Storage and Analysis*. IEEE, 1–15.
- [31] Justin Kalloor, Mathias Weiden, Ed Younis, John Kubiatowicz, Bert De Jong, and Costin Iancu. 2024. Quantum hardware roofline: Evaluating the impact of gate expressivity on quantum processor design. In *2024 IEEE International Conference on Quantum Computing and Engineering (QCE)*, Vol. 1. IEEE, 805–816.
- [32] A Yu Kitaev. 1995. Quantum measurements and the Abelian stabilizer problem. *arXiv preprint quant-ph/9511026* (1995).
- [33] Philip Krantz, Morten Kjaergaard, Fei Yan, Terry P Orlando, Simon Gustavsson, and William D Oliver. 2019. A quantum engineer’s guide to superconducting qubits. *Applied Physics Reviews* 6, 2 (2019), 021318.
- [34] Alon Kukliansky, Ed Younis, Lukasz Cincio, and Costin Iancu. 2023. QFactor: A Domain-Specific Optimizer for Quantum Circuit Instantiation. In *2023 IEEE International Conference on Quantum Computing and Engineering (QCE)*, Vol. 1. IEEE, 814–824.
- [35] Lingling Lao, Hans Van Someren, Imran Ashraf, and Carmen G Almudever. 2021. Timing and resource-aware mapping of quantum circuits to superconducting processors. *IEEE Transactions on Computer-Aided Design of Integrated Circuits and Systems* 41, 2 (2021), 359–371.
- [36] Chris Lattner and Vikram Adve. 2004. LLVM: A Compilation Framework for Lifelong Program Analysis & Transformation. In *Proceedings of the International Symposium on Code Generation and Optimization (CGO)*. IEEE Computer Society, Washington, DC, USA, 75–86. doi:10.1109/CGO.2004.1281665
- [37] Ang Li, Samuel Stein, Sriram Krishnamoorthy, and James Ang. 2023. Qasmbench: A low-level quantum benchmark suite for nisq evaluation and simulation. *ACM Transactions on Quantum Computing* 4, 2 (2023), 1–26.
- [38] Gushu Li, Yufei Ding, and Yuan Xie. 2019. Tackling the qubit mapping problem for NISQ-era quantum devices. In *Proceedings of the twenty-fourth international conference on architectural support for programming languages and operating systems*. 1001–1014.
- [39] Ji Liu, Peiyi Li, and Huiyang Zhou. 2022. Not all swaps have the same cost: A case for optimization-aware qubit routing. In *2022 IEEE International Symposium on High-Performance Computer Architecture (HPCA)*. IEEE, 709–725.
- [40] Ji Liu, Ed Younis, Mathias Weiden, Paul Hovland, John Kubiatowicz, and Costin Iancu. 2023. Tackling the qubit mapping problem with permutation-aware synthesis. In *2023 IEEE International Conference on Quantum Computing and Engineering (QCE)*, Vol. 1. IEEE, 745–756.
- [41] Seth Lloyd. 1996. Universal quantum simulators. *Science* 273, 5278 (1996), 1073–1078.
- [42] Dmitri Maslov. 2007. Linear depth stabilizer and quantum Fourier transformation circuits with no auxiliary qubits in finite-neighbor quantum architectures. *Physical Review A—Atomic, Molecular, and Optical Physics* 76, 5 (2007), 052310.
- [43] Matt McEwen, Dave Bacon, and Craig Gidney. 2023. Relaxing hardware requirements for surface code circuits using time-dynamics. *Quantum* 7 (2023), 1172.
- [44] Evan McKinney and Lev S Bishop. 2025. Two-Qubit Gate Synthesis via Linear Programming for Heterogeneous Instruction Sets. *arXiv preprint arXiv:2505.00543* (2025).
- [45] Evan McKinney, Michael Hatridge, and Alex K Jones. 2024. Mirage: Quantum circuit decomposition and routing collaborative design using mirror gates. In *2024 IEEE International Symposium on High-Performance Computer Architecture (HPCA)*. IEEE, 704–718.
- [46] Long B Nguyen, Yosep Kim, Akel Hashim, Noah Goss, Brian Marinelli, Bibek Bhandari, Debmalaya Das, Ravi K Naik, John Mark Kreikebaum, Andrew N Jordan, et al. 2024. Programmable Heisenberg interactions between Floquet qubits. *Nature Physics* 20, 2 (2024), 240–246.
- [47] Michael A Nielsen and Isaac L Chuang. 2010. *Quantum computation and quantum information*. Cambridge university press.
- [48] Pavel Panteleev and Gleb Kalachev. 2021. Degenerate quantum LDPC codes with good finite length performance. *Quantum* 5 (2021), 585.
- [49] Tirthak Patel, Ed Younis, Costin Iancu, Wibe de Jong, and Devesh Tiwari. 2022. Quest: systematically approximating quantum circuits for higher output fidelity. In *Proceedings of the 27th ACM International Conference on Architectural Support for Programming Languages and Operating Systems*. 514–528.
- [50] Eric C Peterson, Lev S Bishop, and Ali Javadi-Abhari. 2022. Optimal synthesis into fixed xx interactions. *Quantum* 6 (2022), 696.
- [51] Eric C Peterson, Gavin E Crooks, and Robert S Smith. 2020. Fixed-depth two-qubit circuits and the monodromy polytope. *Quantum* 4 (2020), 247.

- [52] Massimiliano Poletto and Vivek Sarkar. 1999. Linear scan register allocation. *ACM Transactions on Programming Languages and Systems (TOPLAS)* 21, 5 (1999), 895–913.
- [53] Timothy Proctor, Kenneth Rudinger, Kevin Young, Erik Nielsen, and Robin Blume-Kohout. 2022. Measuring the capabilities of quantum computers. *Nature Physics* 18, 1 (2022), 75–79.
- [54] Quantinuum. 2024. Native Arbitrary Angle Hardware Gates. https://docs.quantinuum.com/systems/trainings/getting_started/arbitrary_angle_2_qubit_gates.
- [55] Nils Quetschlich, Lukas Burgholzer, and Robert Wille. 2023. MQT Bench: Benchmarking software and design automation tools for quantum computing. *Quantum* 7 (2023), 1062.
- [56] Chad Rigetti and Michel Devoret. 2010. Fully microwave-tunable universal gates in superconducting qubits with linear couplings and fixed transition frequencies. *Physical Review B—Condensed Matter and Materials Physics* 81, 13 (2010), 134507.
- [57] Joschka Roffe, David R White, Simon Burton, and Earl Campbell. 2020. Decoding across the quantum low-density parity-check code landscape. *Physical Review Research* 2, 4 (2020), 043423.
- [58] Peter W Shor. 1994. Algorithms for quantum computation: discrete logarithms and factoring. In *Proceedings 35th annual symposium on foundations of computer science*. Ieee, 124–134.
- [59] Bochen Tan and Jason Cong. 2020. Optimal layout synthesis for quantum computing. In *Proceedings of the 39th International Conference on Computer-Aided Design*. 1–9.
- [60] Jialiang Tang, Jialin Zhang, and Xiaoming Sun. 2024. Quantum circuit synthesis with SQiSW. *arXiv preprint arXiv:2412.14828* (2024).
- [61] Robert R Tucci. 2005. An introduction to Cartan’s KAK decomposition for QC programmers. *arXiv preprint quant-ph/0507171*.
- [62] Ke Wang, Zhide Lu, Chuanyu Zhang, Gongyu Liu, Jiachen Chen, Yanzhe Wang, Yaozu Wu, Shibo Xu, Xuhao Zhu, Feitong Jin, et al. 2025. Demonstration of low-overhead quantum error correction codes. *arXiv preprint arXiv:2505.09684* (2025).
- [63] Ken Xuan Wei, Isaac Lauer, Emily Pritchett, William Shanks, David C McKay, and Ali Javadi-Abhari. 2024. Native two-qubit gates in fixed-coupling, fixed-frequency transmons beyond cross-resonance interaction. *PRX Quantum* 5, 2 (2024), 020338.
- [64] Xin-Chuan Wu, Marc Grau Davis, Frederic T Chong, and Costin Iancu. 2020. QGo: Scalable quantum circuit optimization using automated synthesis. *arXiv preprint arXiv:2012.09835* (2020).
- [65] Christopher G Yale, Ashlyn D Burch, Matthew NH Chow, Brandon P Ruzic, Daniel S Lobser, Brian K McFarland, Melissa C Revelle, and Susan M Clark. 2025. Realization and calibration of continuously parameterized two-qubit gates on a trapped-ion quantum processor. *arXiv preprint arXiv:2504.06259* (2025).
- [66] Christopher G Yale, Rich Rines, Victory Omole, Bharath Thotakura, Ashlyn D Burch, Matthew NH Chow, Megan Ivory, Daniel Lobser, Brian K McFarland, Melissa C Revelle, et al. 2024. Noise-Aware Circuit Compilations for a Continuously Parameterized Two-Qubit Gateset. *arXiv preprint arXiv:2411.01094* (2024).
- [67] Ed Younis, Costin C Iancu, Wim Lavrijsen, Marc Davis, and Ethan Smith. 2021. Berkeley Quantum Synthesis Toolkit (BQSKit). GitHub. doi:10.11578/dc.20210603.2
- [68] Ed Younis, Koushik Sen, Katherine Yelick, and Costin Iancu. 2021. Qfast: Conflating search and numerical optimization for scalable quantum circuit synthesis. In *2021 IEEE International Conference on Quantum Computing and Engineering (QCE)*. IEEE, 232–243.
- [69] Chi Zhang, Ari B Hayes, Longfei Qiu, Yuwei Jin, Yanhao Chen, and Eddy Z Zhang. 2021. Time-optimal qubit mapping. In *Proceedings of the 26th ACM International Conference on Architectural Support for Programming Languages and Operating Systems*. 360–374.
- [70] Jun Zhang, Jiri Vala, Shankar Sastry, and K Birgitta Whaley. 2003. Geometric theory of nonlocal two-qubit operations. *Physical Review A* 67, 4 (2003), 042313.
- [71] Runshi Zhou, Fang Zhang, Linghang Kong, and Jianxin Chen. 2024. Halma: a routing-based technique for defect mitigation in quantum error correction. *arXiv preprint arXiv:2412.21000* (2024).
- [72] Henry Zou, Matthew Treinish, Kevin Hartman, Alexander Ivrii, and Jake Lishman. 2024. Lightsabre: A lightweight and enhanced sabre algorithm. *arXiv preprint arXiv:2409.08368* (2024).
- [73] Alwin Zulehner, Alexandru Paler, and Robert Wille. 2018. An efficient methodology for mapping quantum circuits to the IBM QX architectures. *IEEE Transactions on Computer-Aided Design of Integrated Circuits and Systems* 38, 7 (2018), 1226–1236.
- [74] Alwin Zulehner and Robert Wille. 2019. Compiling SU (4) quantum circuits to IBM QX architectures. In *Proceedings of the 24th Asia and South Pacific Design Automation Conference*. ACM New York, NY, USA, Tokyo, Japan, 185–190.

A Canonical gate and 2Q circuit synthesis

In this section we show the basic mathematical properties of the canonical form of 2Q unitary and then discuss the synthesis capability of some 2Q basis gates.

A.1 Canonical decomposition

$SU(N)$ is a real manifold with dimension $N^2 - 1$, within which any element is a *special unitary* matrix with determinant equal to 1. Since the global phase does not affect quantum computation processes, it is sufficient to focus on the mathematical properties of special unitaries in the area of circuit synthesis. A generic 2Q gate, despite having 15 real parameters, can have its nonlocal behavior fully characterized by only 3 real parameters. This method, known as *Canonical decomposition* or *KAK decomposition* from Lie algebra theory, is widely adopted in quantum computing [8, 61, 70, 74]. Specifically, for any $U \in SU(4)$, there exists a unique $\vec{\eta} = (x, y, z) \in W \subseteq \mathbb{R}^3$, along with $V_1, V_2, V_3, V_4 \in SU(2)$ and a global phase, such that

$$U = g \cdot (V_1 \otimes V_2) e^{-i\vec{\eta} \cdot \vec{\Sigma}} (V_3 \otimes V_4), \quad g \in \{1, i\} \quad (5)$$

where $\vec{\Sigma} \equiv (XX, YY, ZZ)$ [61]. The set

$$W := \left\{ (x, y, z) \in \mathbb{R}^3 \mid \frac{\pi}{4} \geq x \geq y \geq |z|, z \geq 0 \text{ if } x = \frac{\pi}{4} \right\} \quad (6)$$

is known as the *Weyl chamber* [70], and $\vec{\eta} \in W$ is known as the *Weyl coordinate* of U . We also refer to a gate of the form

$$\text{Can}(a, b, c) := e^{-i\frac{\pi}{2}(aXX+bYY+cZZ)} = \begin{pmatrix} e^{-i\frac{c\pi}{2}} \cos \frac{(a-b)\pi}{2} & 0 & 0 & -ie^{-i\frac{c\pi}{2}} \sin \frac{(a-b)\pi}{2} \\ 0 & e^{i\frac{c\pi}{2}} \cos \frac{(a+b)\pi}{2} & -ie^{i\frac{c\pi}{2}} \sin \frac{(a+b)\pi}{2} & 0 \\ 0 & -ie^{i\frac{c\pi}{2}} \sin \frac{(a+b)\pi}{2} & e^{i\frac{c\pi}{2}} \cos \frac{(a+b)\pi}{2} & 0 \\ -ie^{-i\frac{c\pi}{2}} \sin \frac{(a-b)\pi}{2} & 0 & 0 & e^{-i\frac{c\pi}{2}} \cos \frac{(a-b)\pi}{2} \end{pmatrix} \quad (7)$$

as a *canonical gate*. Two 2Q gates U and V are considered *locally equivalent* if they differ only by 1Q gates, meaning their canonical coefficients can be transformed into one another via the equivalence rules [15]:

1. $(a, b, c) \sim (b, a, c)$ or $(a, b, c) \sim (c, b, a)$, i.e., any permutation of the coefficients;
2. $(a, b, c) \sim (-a, -b, c)$;
3. $(a, b, c) \sim (a - 1, b, c)$;
4. $(1/2, b, c) \sim (1/2, b, -c)$.

Note that we align the conventional that canonical coefficient (a, b, c) differs from Weyl coordinate (x, y, z) by a $\frac{\pi}{2}$ factor. Unless otherwise specified, the canonical coefficients of gates in quantum ISAs and circuits are confined to $\frac{1}{2} \geq a \geq b \geq |c|$. While for the Weyl chamber visualization by means of `weylchamber` [21], we assume the Weyl coordinates are confined to $\{\frac{\pi}{4} \geq x \geq y \geq z \geq 0\} \cup \{\frac{\pi}{4} \geq \frac{\pi}{2} - x \geq y \geq z \geq 0\}$, as illustrated by Figure 3. Conversion of Weyl coordinates for different conventions is simple according to the equivalence rules above.

A.2 Quantum ISA and the synthesis capability

A quantum ISA typically includes qubit initialization, a universal gate set, and measurement. It serves as an interface between software and hardware by mapping high-level semantics of quantum programs to low-level native quantum operations or pulse sequences on hardware. The universal gate set, especially specified by its 2Q basis gates, is the key component of a quantum ISA that dominates its hardware-implementation accuracy and cost, as well as software-expressivity sufficiency.

CX or CNOT is the most popular basis gate provides by hardware vendors and considered by various quantum compiler optimization methods. The superconducting Cross-Resonance gate [56] and ion-trapped Mølmer-Sørensen gate [7] are both CX-equivalent gates with the same canonical form $\text{Can}(\frac{1}{2}, 0, 0)$. In the superconducting platforms with XY -coupled Hamiltonian like Google's Sycamore [4], $i\text{SWAP} \sim \text{Can}(\frac{1}{2}, \frac{1}{2}, 0)$ is another representative native 2Q basis gate and could be less sensitive to

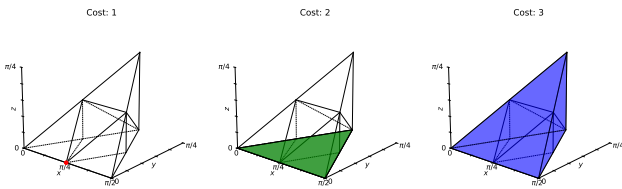


Figure 12. Coverage set for CX ISA.

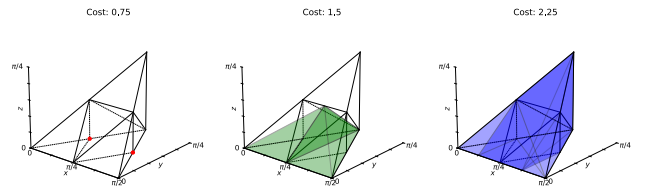


Figure 13. Coverage set for SqISW ISA.

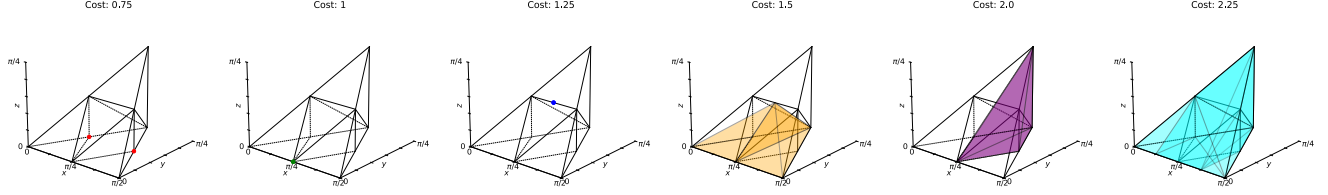


Figure 14. Coverage set for SQiSW_ISA.

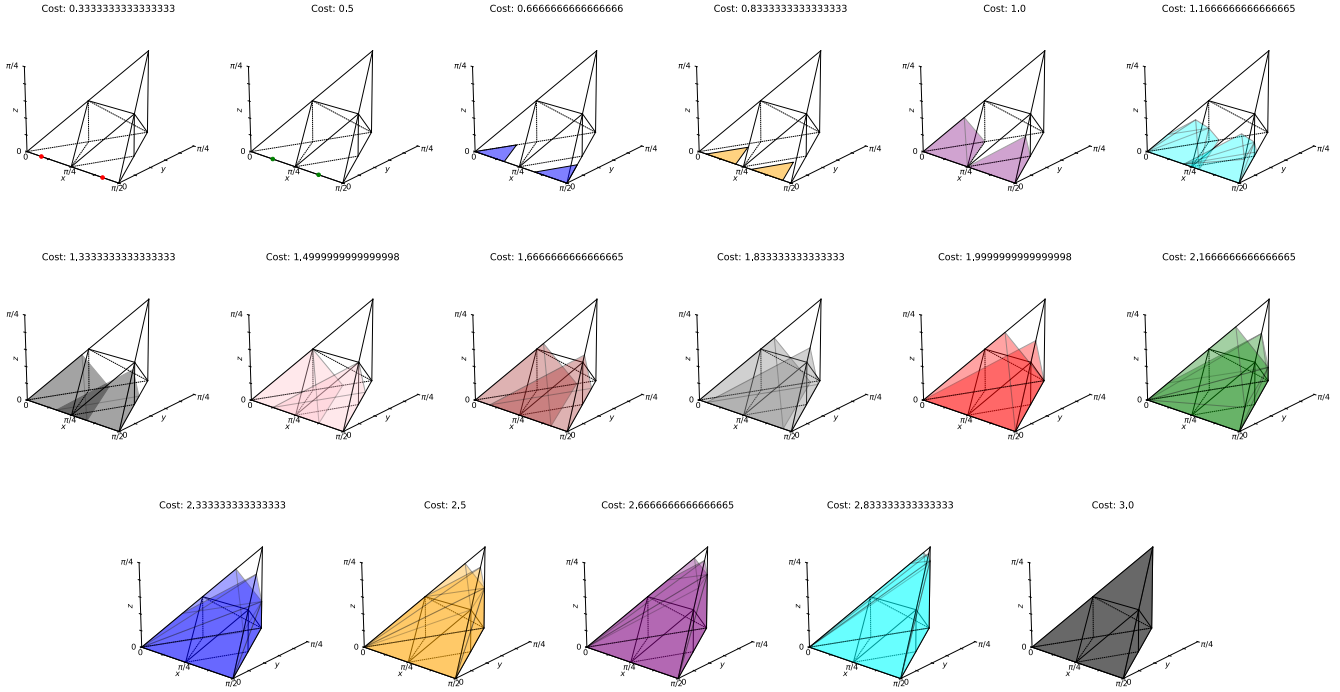


Figure 15. Coverage set for ZZPhase ISA.

leakage error than the native CZ gate. Recent experimental advances demonstrate that more basis gates could be implemented natively and calibrated in high precision [12, 63, 65]. Particularly, some basis gates like \sqrt{i} SWAP $\sim \text{Can}(\frac{1}{4}, \frac{1}{4}, 0)$ and fractional ZZ(θ) $\sim \text{Can}(a, 0, 0)$ gates offers more promising ISA selections as they exhibit shorter gate duration, higher gate accuracy, and stronger synthesis capability.

The synthesis capability or computational power of basis gates can be geometrically illustrated by monodrome polytopes within the Weyl chamber. The coverage set for CX depicted in Figure 12 implies that

1. One CX gate is required to synthesize 2Q gates $\sim \text{Can}(\frac{1}{2}, 0, 0)$, i.e., CX-equivalent gates $(V_1 \otimes V_2)CX(V_3 \otimes V_4)$;
2. Two CX gates are required to synthesize 2Q gates $\sim \text{Can}(a, b, 0)$, i.e., $(V_1 \otimes V_2)CX(V_3 \otimes V_4)CX(V_5 \otimes V_6)$;
3. Three CX gates are required to synthesize 2Q gates $\sim \text{Can}(a, b, c)$, i.e., $(V_1 \otimes V_2)CX(V_3 \otimes V_4)CX(V_5 \otimes V_6)CX(V_7 \otimes V_8)$.

We assume the cost of one CX gate is 1.0. Polytopes in different colors denotes the minimal circuit cost (duration) for the coverage set if synthesized by CX and arbitrary 1Q gates. That is, on average, the number of CX gates required to synthesize arbitrary 2Q gates is 3. In contrast, the number for SQiSW ISA is 2.21 [26].

Monodromy polytope theory [51] provides a framework for determining the synthesis coverage set and circuit cost (in 2Q depth) for any set of basis gates with specified costs, while the specific gate decomposition process is left to the synthesizer to complete. For the selected ISAs in Table 2 with the basis gate costs assumed in Equation (4), Figures 12 to 17 describes their coverage sets, respectively. With the enrichment of quantum ISA (e.g., combining gate families, involving mirror gates) and heterogeneous basis gate cost settings, the coverage set reveals a richer variety of convex polyhedra. That implies more optimization effects for the ISA-ware routing mechanism in CANOPUS.

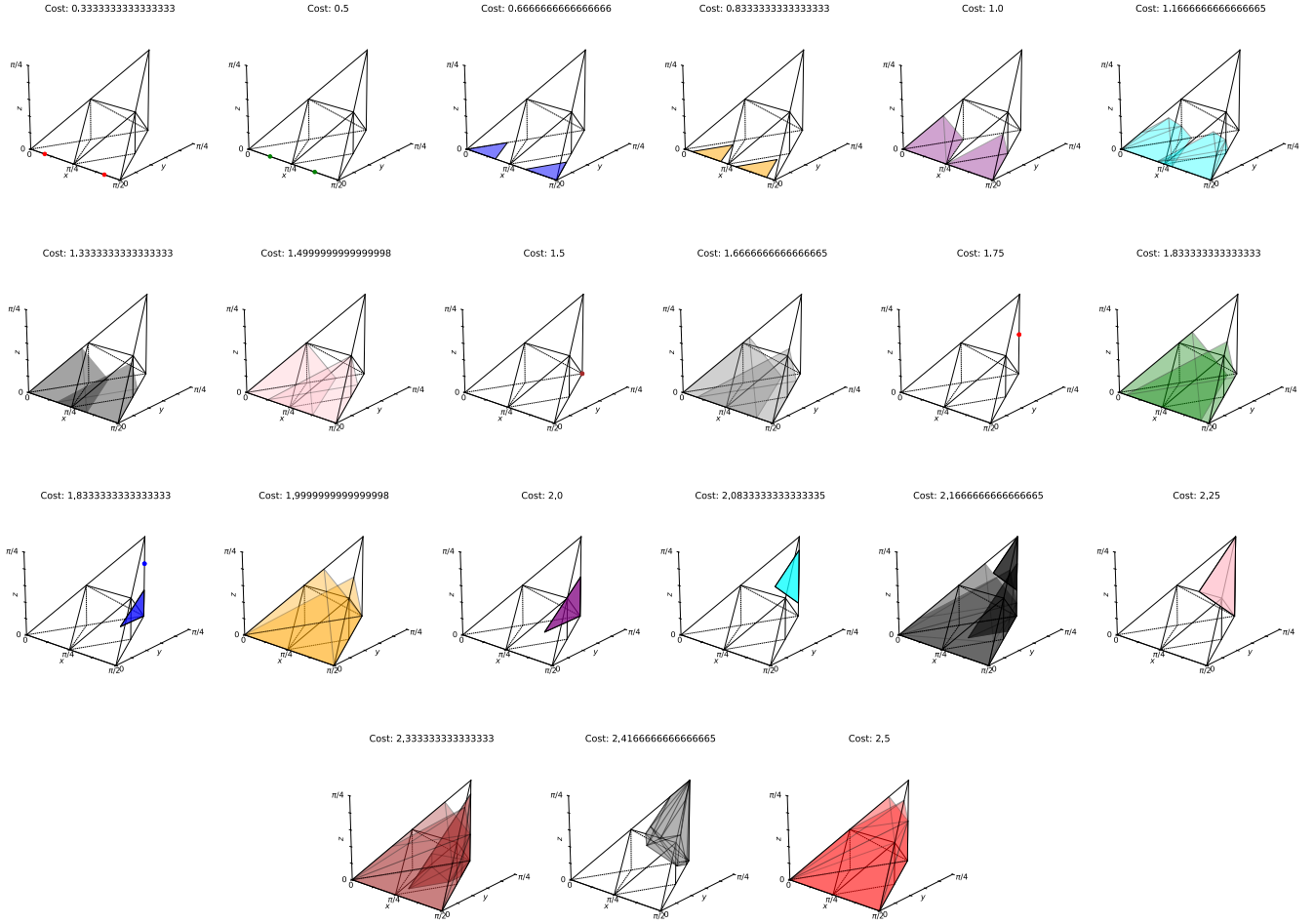
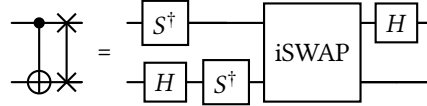


Figure 16. Coverage set for ZZPhase_ISA.

A.3 2Q gate mirroring

The mirror symmetry of a 2Q gate U is defined as the composition of the original gate and a SWAP gate [53], i.e., $\text{SWAP} \cdot U$. For example, CX and iSWAP is a typical pair of mirror gates as shown below.



In general, the mirroring rule for Canonical coefficients is described as

$$\text{SWAP} \cdot \text{Can}(a, b, c) \sim \left(a + \frac{1}{2}, b + \frac{1}{2}, c + \frac{1}{2}\right) \sim \left(a + \frac{1}{2} - 1, b + \frac{1}{2} - 1, c + \frac{1}{2} - 1\right) \sim \begin{cases} \left(\frac{1}{2} - c, \frac{1}{2} - b, a - \frac{1}{2}\right), & \text{if } c \geq 0 \\ \left(\frac{1}{2} + c, \frac{1}{2} - b, \frac{1}{2} - a\right), & \text{if } c < 0 \end{cases} \quad (8)$$

The mirror pair of CX and iSWAP is a special case implying that a CX-iSWAP combination ISA could result in lower overhead in routing-synthesis collaborative optimization. Yale et al. [66] once considers inserting SWAP gates to get mirrored gates with lower synthesis overhead compared to the original gates, given the all-to-all topology and continuous $\text{ZZ}(\theta)$ gate set on ion-trapped hardware. McKinney et al. [45] discusses that integrating $\sqrt{\text{iSWAP}}$'s mirror gate, i.e., $\text{ECP} \sim \text{Can}\left(\frac{1}{4}, \frac{1}{4}, 0\right)$ gate, into the powerful SqISW ISA, could further improve the ISA's synthesis capability and end-to-end routing-synthesis co-optimization on limited topologies.

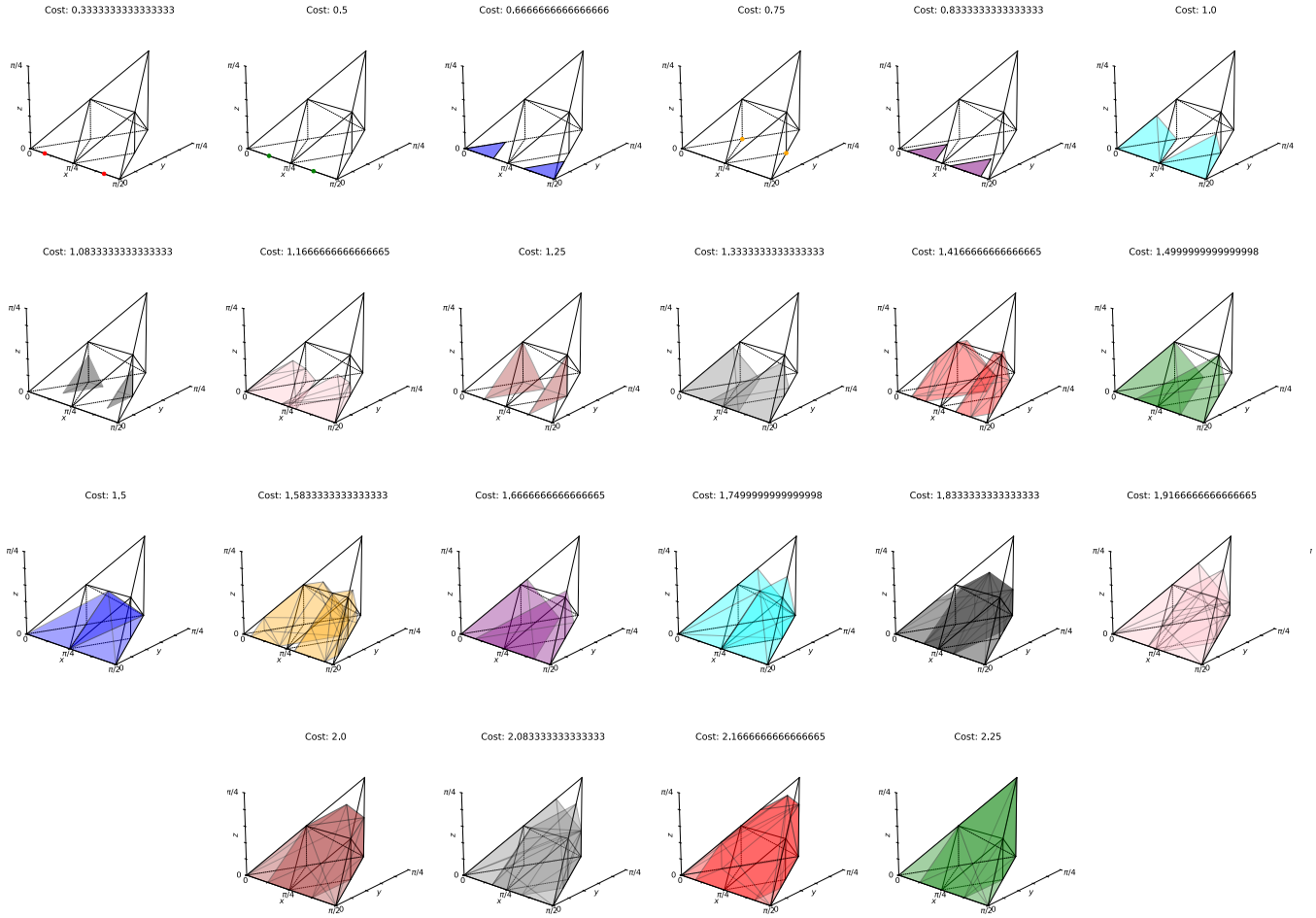


Figure 17. Coverage set for Het ISA.

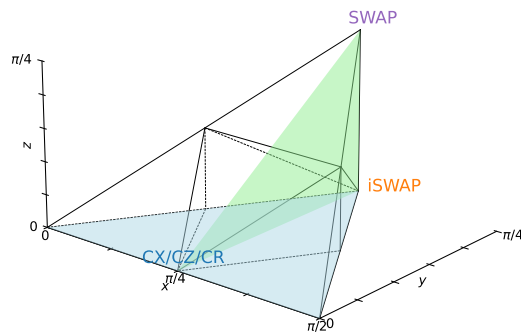


Figure 18. Morrir symmetry for $\text{Can}(a, b, 0)$ and $\text{Can}(\frac{1}{2}, b', c')$ gate families.

B Commutative relation of canonical gates

Herein we present detailed proof for Theorem 1. The *if* direction is trivial, and hence we justify the *only if* direction, relying on the following two lemmas.

Lemma 1. *Let A, B be two Hermitian matrices with eigenvalues in the range $[-2, 2]$. If $[e^{-i\frac{\pi}{2}A}, e^{-i\frac{\pi}{2}B}] = 0$ then $[A, B] = 0$.*

Proof. This follows from the fact that compatible observables (commuting operators) can be simultaneously diagonalized. In this case, the respective unitary matrix $e^{-i\frac{\pi}{2}A}$ commutes with $e^{-i\frac{\pi}{2}B}$. Denote by A_λ the eigenspace corresponding to the eigenvalue λ of $e^{-i\frac{\pi}{2}A}$, i.e. $e^{-i\frac{\pi}{2}A} = \oplus_\lambda \lambda A_\lambda$. Then we have

$$\forall \vec{v} \in A_\lambda, e^{-i\frac{\pi}{2}B} e^{-i\frac{\pi}{2}A} \vec{v} = e^{-i\frac{\pi}{2}B} \lambda \vec{v} = \lambda e^{-i\frac{\pi}{2}B} \vec{v} = e^{-i\frac{\pi}{2}A} e^{-i\frac{\pi}{2}B} \vec{v}, \quad (9)$$

and thus $e^{-i\frac{\pi}{2}B} \vec{v} \in A_\lambda$. Thus A_λ is $e^{-i\frac{\pi}{2}B}$ -invariant and the restriction $e^{-i\frac{\pi}{2}B}|_{A_\lambda}$ of $e^{-i\frac{\pi}{2}B}$ to A_λ is still unitary since it preserves inner products. Hence it is diagonalizable and we can find an orthonormal basis $w_{\lambda_1}, w_{\lambda_2}, \dots, w_{\lambda_k}$ consisting of eigenvectors of $e^{-i\frac{\pi}{2}B}|_{A_\lambda}$. Note that these are also eigenvectors of $e^{-i\frac{\pi}{2}A}$ (with eigenvalue λ). Following the same token as above, for each eigenspace E_{λ_i} of $e^{-i\frac{\pi}{2}A}$, we can construct an orthonormal basis β_i for it consisting of eigenvectors of $e^{-i\frac{\pi}{2}B}$. Finally since the eigenspaces of different eigenvalues of $e^{-i\frac{\pi}{2}A}$ are orthogonal to each other, $\beta = \cup_i \beta_i$ forms an orthonormal basis of the entire Hilbert space \mathcal{H}_n consisting of the coeigenvectors of both $e^{-i\frac{\pi}{2}A}$ and $e^{-i\frac{\pi}{2}B}$.

Now let U be a unitary matrix with the vectors in β being its columns, then

$$\begin{aligned} U^\dagger e^{-i\frac{\pi}{2}A} U &= D_A \\ U^\dagger e^{-i\frac{\pi}{2}B} U &= D_B \end{aligned} \quad (10)$$

In general, an eigenvector of $e^{-i\frac{\pi}{2}A}$ need *not* be that of A . However, since A has its eigenvalues in the range $[-2, 2)$, the map

$$f : [-2, 2) \rightarrow U(1), a \rightarrow e^{-i\frac{\pi}{2}a} \quad (11)$$

is injective. Consequently different eigenvalues of A correspond to different eigenvalues of $e^{-i\frac{\pi}{2}A}$, and hence the eigenspaces of $e^{-i\frac{\pi}{2}A}$ and A coincide. Therefore, we have that

$$\begin{aligned} U^\dagger A U &= \Sigma_A \\ U^\dagger B U &= \Sigma_B \end{aligned} \quad (12)$$

and since $[\Sigma_A, \Sigma_B] = 0$ as they are diagonal, $[A, B] = 0$. We obtain the desired result. \square

Lemma 2. Let $P_1 = (a_1 X_1 X_2 + b_1 Y_1 Y_2 + c_1 Z_1 Z_2) I_3$, $P_2 = I_1 (a_2 X_2 X_3 + b_2 Y_2 Y_3 + c_2 Z_2 Z_3)$ with $|c_1| \leq b_1 \leq a_1 \leq \frac{1}{2}$, $|c_2| \leq b_2 \leq a_2 \leq \frac{1}{2}$. If $[P_1, P_2] = 0$ and $P_1, P_2 \neq 0$, then $b_1 = b_2 = c_1 = c_2 = 0$.

Proof. Consider the product $P_1 P_2$. We assume for the sake of contradiction that $b_1 \neq 0$. Using $[X, Y] = 2iZ$, $[Y, Z] = 2iX$, $[Z, X] = 2iY$, we expand

$$[P_1, P_2] = 2i(a_1 b_2 X_1 Z_2 Y_3 - b_1 a_2 Y_1 Z_2 X_3 + b_1 c_2 Y_1 X_2 Z_3) - 2i(a_1 c_2 X_1 Y_2 Z_3 + c_1 a_2 Z_1 Y_2 X_3 + c_1 b_2 Z_1 X_2 Y_3).$$

Since the each Pauli string is linearly independent in the 8×8 operator basis, e.g. term $Y_1 Z_2 X_3$ cannot be canceled out by any other terms, contradictory to the fact that $[P_1, P_2] = 0$. Hence, vanishing of $[P_1, P_2]$ requires

$$a_1 b_2 = a_1 c_2 = b_1 c_2 = b_1 a_2 = c_1 a_2 = c_1 b_2 = 0.$$

Since $P_1, P_2 \neq 0$, at least a_1, a_2 is nonzero, leading to $b_1 = b_2 = c_1 = c_2 = 0$. \square

Using Lemma 1 and Lemma 2 above, it is straightforward to prove Theorem 1. We see that $\|P_1\| \leq \|a_1 X_1 X_2 I_3\| + \|b_1 Y_1 Y_2 I_3\| + \|c_1 Z_1 Z_2 I_3\| \leq |a_1| + |b_1| + |c_1| \leq \frac{3}{2}$, where $\|\cdot\|$ is the operator norm. Hence, eigenvalues of P_1 are in range of $[-2, 2)$. Same as the eigenvalues of P_2 . Now if $[e^{-i\frac{\pi}{2}P_1}, e^{-i\frac{\pi}{2}P_2}] = 0$, then we have that $[P_1, P_2] = 0$ according to Lemma 1, and thus $b_1 = b_2 = c_1 = c_2 = 0$ according to Lemma 2, which proves the *only if* direction.

C Detailed evaluation results

Table 5. Routing overhead in terms of C_{count} for different compilers across different topologies and quantum ISAs.

Chain	CX ISA				ZZPhase ISA				SqISW ISA				ZZPhase_ ISA				SqISW_ ISA				Het ISA						
	sabre	toqm	bqskit	canop	sabre	toqm	bqskit	canop	sabre	toqm	bqskit	canop	sabre	toqm	bqskit	canop	sabre	toqm	bqskit	canop	sabre	toqm	bqskit	canop	sabre	toqm	bqskit
bigadd	2.53	2.44	1.59	1.92	2.35	2.26	1.53	1.97	2.39	2.23	1.42	1.98	1.90	1.81	1.57	1.59	1.94	1.85	1.49	1.57	1.95	1.85	1.31	1.77			
bv	2.67	4.06	10.94	2.00	2.67	4.06	10.94	2.33	2.38	3.12	8.12	1.88	2.09	3.01	8.12	1.63	2.03	2.89	7.22	1.61	2.12	3.07	7.76	1.79			
ising	1.00	1.00	1.00	1.00	0.38	0.38	0.38	0.38	0.75	0.75	0.75	0.75	0.38	0.38	0.38	0.38	0.75	0.75	0.75	0.75	0.38	0.38	0.38	0.38			
knn	2.60	4.02	1.48	1.29	2.40	3.93	1.22	1.23	2.43	3.46	1.21	1.39	1.93	3.01	1.13	1.04	1.98	2.90	1.06	1.07	1.98	3.11	1.01	1.08			
multi	2.32	4.97	2.53	2.68	2.18	4.83	2.28	2.49	2.26	4.17	1.99	2.38	1.79	3.67	1.84	2.02	1.81	3.56	1.73	2.04	1.83	3.78	1.68	2.01			
qec9	4.44	12.34	6.88	3.56	4.44	12.34	5.33	3.53	3.89	9.52	3.47	2.84	3.43	9.05	5.23	2.77	3.25	8.45	3.98	2.56	3.52	9.34	4.27	2.77			
qft	1.74	1.50	1.78	1.49	1.51	1.45	2.02	1.45	1.31	1.12	1.53	1.12	1.12	1.05	1.50	1.05	1.19	1.00	1.32	1.00	1.16	1.10	1.41	1.10			
qpe	2.77	3.32	3.15	2.86	2.46	3.09	2.89	2.75	2.08	2.50	2.23	2.13	1.82	2.27	2.07	1.99	1.89	2.24	2.13	1.88	1.89	2.36	2.35	2.04			
qram	2.94	5.37	2.75	3.23	2.75	5.21	2.73	3.02	2.63	4.44	2.53	2.80	2.16	3.93	2.29	2.45	2.19	3.80	2.22	2.37	2.22	4.06	2.26	2.43			
sat	2.44	2.66	1.88	2.29	2.23	2.43	1.38	2.13	2.24	2.36	1.42	2.03	1.79	1.92	1.39	1.67	1.85	1.99	1.32	1.76	1.83	1.96	1.13	1.73			
swapt	2.87	4.02	1.43	1.29	2.67	3.93	1.22	1.23	2.66	3.46	1.21	1.39	2.13	3.01	1.02	1.10	2.17	2.90	1.07	1.07	2.19	3.11	1.00	1.08			
wstate	1.00	1.00	1.00	1.00	1.00	1.00	0.99	1.00	1.50	1.50	1.47	1.50	1.00	1.00	0.99	1.00	1.00	0.99	1.00	1.00	1.00	1.00	0.99	1.00			
Avg.	2.26	3.07	2.27	1.88	1.97	2.75	1.92	1.7	2.06	2.63	1.85	1.73	1.61	2.18	1.69	1.39	1.72	2.25	1.68	1.45	1.65	2.23	1.58	1.43			
HHex	CX ISA				ZZPhase ISA				SqISW ISA				ZZPhase_ ISA				SqISW_ ISA				Het ISA						
	sabre	toqm	bqskit	canop	sabre	toqm	bqskit	canop	sabre	toqm	bqskit	canop	sabre	toqm	bqskit	canop	sabre	toqm	bqskit	canop	sabre	toqm	bqskit	canop	sabre	toqm	bqskit
bigadd	2.17	2.10	1.90	1.89	2.00	1.93	2.35	1.92	2.14	2.02	1.86	1.84	1.65	1.58	1.24	1.45	1.70	1.63	1.57	1.45	1.69	1.61	1.33	1.53			
bv	3.28	2.22	7.22	1.94	3.28	2.22	7.23	1.83	3.00	2.12	5.83	1.50	2.58	1.80	5.51	1.51	2.47	1.75	4.94	1.42	2.64	1.82	5.35	1.68			
ising	1.72	3.20	1.64	1.42	1.10	2.77	0.83	0.83	1.29	2.50	1.17	1.11	0.90	2.12	0.84	0.67	1.23	2.24	1.15	1.04	0.92	2.18	0.86	0.58			
knn	2.18	2.57	2.17	1.49	1.98	2.43	1.81	1.39	2.12	2.33	1.91	1.54	1.63	1.92	1.61	1.16	1.70	1.93	1.66	1.25	1.66	1.97	1.75	1.17			
multi	2.23	3.48	2.11	2.24	2.09	3.35	1.69	2.10	2.19	3.07	1.95	2.00	1.72	2.61	1.64	1.64	1.75	2.57	1.70	1.75	1.75	2.68	1.53	1.67			
qec9	3.16	4.78	4.84	3.16	3.16	4.78	4.82	3.19	2.91	4.03	4.20	2.84	2.49	3.64	3.81	2.43	2.39	3.45	4.94	2.39	2.55	3.73	5.23	2.53			
qft	1.91	2.62	2.44	1.67	1.60	2.35	1.83	1.52	1.43	1.97	1.61	1.27	1.19	1.73	1.50	1.12	1.31	1.78	1.46	1.12	1.24	1.80	1.59	1.16			
qpe	2.58	2.90	2.89	2.43	2.15	2.59	2.44	2.10	1.94	2.18	2.30	1.86	1.61	1.92	1.96	1.62	1.77	1.97	1.86	1.68	1.67	1.99	1.82	1.67			
qram	2.52	4.32	3.03	2.42	2.32	4.15	3.23	2.31	2.35	3.68	2.52	2.19	1.87	3.17	2.58	1.86	1.92	3.11	2.18	1.85	1.91	3.27	1.94	1.87			
sat	2.27	2.29	1.60	2.00	2.05	2.06	1.28	1.81	2.10	2.10	1.35	1.83	1.65	1.66	1.33	1.44	1.74	1.74	1.26	1.52	1.69	1.69	1.03	1.49			
swapt	2.24	2.57	2.06	1.50	2.04	2.43	1.78	1.42	2.18	2.33	1.98	1.56	1.68	1.92	1.63	1.14	1.74	1.93	2.20	1.21	1.71	1.97	1.82	1.18			
wstate	2.65	2.04	2.60	1.69	2.65	2.04	2.47	1.46	2.71	2.28	2.21	1.67	2.19	1.75	2.07	1.50	2.10	1.69	1.78	1.35	2.23	1.78	1.97	1.60			
Avg.	2.37	2.82	2.59	1.93	2.12	2.65	2.25	1.74	2.14	2.48	2.17	1.72	1.7	2.08	1.88	1.4	1.78	2.09	1.98	1.46	1.74	2.13	1.86	1.43			
Square	CX ISA				ZZPhase ISA				SqISW ISA				ZZPhase_ ISA				SqISW_ ISA				Het ISA						
	sabre	toqm	bqskit	canop	sabre	toqm	bqskit	canop	sabre	toqm	bqskit	canop	sabre	toqm	bqskit	canop	sabre	toqm	bqskit	canop	sabre	toqm	bqskit	canop	sabre	toqm	bqskit
bigadd	1.62	1.89	1.41	1.38	1.44	1.71	1.02	1.18	1.75	1.92	1.42	1.43	1.26	1.44	1.17	1.04	1.34	1.51	1.23	1.14	1.27	1.46	1.10	1.02			
bv	2.72	2.22	4.39	1.50	2.72	2.22	4.39	1.50	2.75	2.38	3.67	1.50	2.23	1.87	3.44	1.22	2.14	1.81	2.94	1.31	2.28	1.90	3.17	1.22			
ising	1.00	1.00	1.78	1.00	0.38	0.38	1.16	0.38	0.75	0.75	1.33	0.75	0.38	0.38	0.90	0.38	0.75	0.75	1.27	0.75	0.38	0.38	0.96	0.38			
knn	1.79	2.64	1.88	1.29	1.57	2.43	1.52	1.23	1.88	2.46	1.59	1.42	1.35	1.96	1.40	1.04	1.45	2.01	1.46	1.07	1.38	2.00	1.28	1.05			
multi	1.84	2.81	1.99	1.56	1.68	2.67	1.49	1.42	1.95	2.64	1.64	1.58	1.44	2.14	1.32	1.24	1.50	2.14	1.64	1.28	1.47	2.19	1.21	1.26			
qec9	2.06	4.44	3.69	1.78	2.06	4.44	3.80	1.72	2.20	3.89	2.88	1.71	1.74	3.43	2.30	1.44	1.69	3.25	2.34	1.50	1.77	3.52	2.42	1.46			
qft	1.41	2.30	2.09	1.35	1.03	1.88	1.41	1.05	1.06	1.75	1.50	1.00	0.79	1.42	1.08	0.80	0.99	1.60	1.37	0.94	0.82	1.47	1.06	0.81			
qpe	1.68	2.50	2.06	1.46	1.22	2.00	1.42	1.18	1.26	1.91	1.47	1.11	0.95	1.53	1.08	0.93	1.18	1.74	1.48	0.99	0.98	1.58	1.26	0.90			
qram	1.88	2.67	2.40	1.60	1.65	2.48	1.78	1.44	1.88	2.48	2.00	1.55	1.39	1.99	1.70	1.22	1.50	2.02	1.74	1.27	1.41	2.04	1.47	1.29			
sat	1.65	2.09	1.44	1.54	1.42	1.87	1.22	1.34	1.70	2.06	1.25	1.45	1.22	1.55	1.11	1.11	1.34	1.64	1.14	1.21	1.24	1.58	0.94	1.12			
swapt	1.75	2.64	2.06	1.29	1.54	2.43	1.14	1.18	1.85	2.46	1.46	1.44	1.33	1.96	1.38	1.04	1.43	2.01	1.47	1.11	1.35	2.00	1.33	1.07			
wstate	1.00	1.00	1.25	1.00	1.00	1.00	1.39	1.00	1.50	1.50	1.82	1.50	1.00	1.00	1.53	1.00	1.00	1.00	1.31	1.00	1.00	1.00	1.32	1.00			
Avg.	1.64	2.18	2.06	1.38	1.35	1.87	1.61	1.16	1.63	2.05	1.74	1.34	1.16	1.55	1.43	0.99	1.31	1.69	1.56	1.11	1.18	1.58	1.36	1.0			

Table 6. Routing overhead in terms of C_{depth} for different compilers across different topologies and quantum ISAs.

Chain	CX ISA				ZZPhase ISA				SQiSW ISA				ZZPhase_ ISA				SQiSW_ ISA				Het ISA			
	sabre	toqm	bqskit	canop	sabre	toqm	bqskit	canop	sabre	toqm	bqskit	canop	sabre	toqm	bqskit	canop	sabre	toqm	bqskit	canop	sabre	toqm	bqskit	canop
bigadd	2.82	1.95	1.45	1.73	2.66	1.81	1.27	1.81	2.65	1.88	1.40	1.88	2.14	1.48	1.16	1.48	2.15	1.53	1.30	1.48	2.19	1.51	1.05	1.46
bv	2.83	2.72	5.06	2.11	2.83	2.72	5.06	2.39	2.62	2.12	4.12	2.12	2.26	2.01	3.73	1.74	2.19	1.89	3.58	1.72	2.29	2.07	3.99	1.85
ising	1.00	1.00	1.00	1.00	0.46	0.46	0.46	0.46	0.75	0.75	0.75	0.75	0.46	0.46	0.46	0.46	0.75	0.75	0.75	0.75	0.46	0.46	0.46	0.46
knn	3.16	2.66	1.65	1.39	2.90	2.53	1.45	1.31	2.76	2.32	1.35	1.35	2.27	1.95	1.32	1.05	2.32	1.95	1.17	1.10	2.33	2.03	1.12	1.11
multi	2.33	3.49	2.45	2.17	2.23	3.41	2.14	1.93	2.28	3.06	1.88	1.88	1.96	1.82	2.64	1.89	1.64	1.82	2.56	1.57	1.59	1.86	2.71	1.58
qec9	5.33	7.33	6.00	4.08	5.33	7.33	5.58	3.83	4.38	5.75	4.00	3.38	4.00	5.40	4.70	3.36	3.75	5.04	4.33	2.79	4.12	5.58	4.75	3.29
qft	2.85	1.50	2.50	1.50	1.95	1.43	3.02	1.42	2.14	1.12	2.24	1.12	1.53	1.04	2.27	1.03	2.01	1.01	2.02	1.01	1.58	1.08	2.29	1.08
qpe	4.00	2.97	3.66	2.83	3.32	2.69	3.67	2.77	3.00	2.23	2.73	2.12	2.49	1.99	2.62	1.83	2.75	2.01	2.64	1.90	2.58	2.06	2.70	1.71
qram	2.04	3.79	2.45	2.50	2.80	3.73	2.24	2.24	2.64	3.21	2.16	2.28	2.21	2.84	2.03	1.90	2.19	2.72	2.03	1.91	2.27	2.93	1.76	1.94
sat	2.28	2.00	1.77	1.88	2.12	1.85	1.25	1.64	2.19	1.87	1.30	1.75	1.73	1.50	1.36	1.37	1.77	1.54	1.20	1.48	1.77	1.52	1.06	1.38
swapt	3.42	2.66	1.58	1.39	3.15	2.53	1.44	1.31	2.98	2.32	1.37	1.35	2.45	1.95	1.12	1.13	2.50	1.95	1.16	1.10	2.52	2.03	1.11	1.11
wstate	1.00	1.00	1.04	1.00	1.00	1.00	1.02	1.00	1.50	1.50	1.50	1.50	1.00	1.00	1.02	1.00	1.00	1.00	1.02	1.00	1.00	1.00	1.01	1.00
Avg.	2.57	2.38	2.18	1.81	2.22	2.15	1.91	1.63	2.32	2.08	1.84	1.68	1.82	1.72	1.66	1.35	1.95	1.76	1.66	1.4	1.86	1.76	1.56	1.36
HHex	CX ISA				ZZPhase ISA				SQiSW ISA				ZZPhase_ ISA				SQiSW_ ISA				Het ISA			
	sabre	toqm	bqskit	canop	sabre	toqm	bqskit	canop	sabre	toqm	bqskit	canop	sabre	toqm	bqskit	canop	sabre	toqm	bqskit	canop	sabre	toqm	bqskit	canop
bigadd	2.55	1.77	1.81	1.80	2.39	1.62	2.12	1.80	2.46	1.78	1.59	1.69	1.95	1.37	1.32	1.32	1.97	1.43	1.56	1.35	1.99	1.38	1.19	1.34
bv	3.06	2.11	3.28	2.00	3.06	2.11	3.28	1.89	2.79	1.96	2.79	1.58	2.41	1.69	2.51	1.56	2.31	1.64	2.33	1.53	2.46	1.71	2.52	1.85
ising	4.50	6.25	4.25	3.00	3.58	5.92	2.71	2.12	3.38	5.25	2.44	2.62	2.75	4.54	2.42	1.60	3.12	4.50	2.88	2.62	2.83	4.67	2.44	1.19
knn	2.52	2.19	1.94	1.48	2.24	2.01	1.68	1.35	2.30	2.02	1.90	1.56	1.80	1.60	1.49	1.09	1.90	1.66	1.69	1.30	1.84	1.65	1.56	1.19
multi	2.14	2.76	1.88	1.92	2.05	2.69	1.50	1.80	2.11	2.51	1.82	1.93	1.68	2.12	1.57	1.54	1.68	2.06	1.59	1.75	1.71	2.17	1.41	1.57
qec9	4.50	3.83	4.25	3.25	4.50	3.83	4.29	3.42	4.06	3.38	5.25	3.06	3.51	2.96	3.29	2.64	3.33	2.83	5.38	2.75	3.60	3.02	5.77	3.08
qft	3.56	3.62	3.80	2.42	2.87	3.18	2.78	2.34	2.67	2.73	2.44	1.78	2.16	2.36	2.34	1.84	2.46	2.48	2.43	1.51	2.23	2.44	2.55	1.85
qpe	4.53	2.98	4.13	2.97	3.67	2.64	3.37	2.52	3.41	2.26	3.43	2.48	2.77	1.97	2.76	1.83	3.14	2.03	2.49	2.38	2.87	2.04	2.29	1.90
qram	2.86	3.01	2.87	2.17	2.67	2.84	2.44	1.92	2.66	2.71	2.16	2.04	2.15	2.25	2.26	1.74	2.17	2.24	2.02	1.62	2.20	2.30	2.02	1.80
sat	2.18	1.84	1.48	1.77	2.03	1.69	1.17	1.62	2.09	1.81	1.28	1.68	1.65	1.40	1.27	1.33	1.70	1.46	1.18	1.39	1.69	1.42	0.95	1.36
swapt	2.47	2.19	2.00	1.53	2.19	2.01	1.64	1.34	2.25	2.02	1.79	1.58	1.76	1.60	1.51	1.13	1.86	1.66	1.77	1.17	1.80	1.65	1.68	1.21
wstate	3.07	1.93	2.43	1.57	3.07	1.93	2.02	1.57	3.03	2.25	2.41	2.04	2.49	1.69	1.86	1.65	2.38	1.64	1.89	1.36	2.54	1.71	2.07	1.42
Avg.	3.05	2.68	2.66	2.08	2.77	2.52	2.26	1.91	2.71	2.43	2.28	1.96	2.2	2.0	1.96	1.56	2.27	2.02	2.1	1.66	2.25	2.05	1.98	1.58
Square	CX ISA				ZZPhase ISA				SQiSW ISA				ZZPhase_ ISA				SQiSW_ ISA				Het ISA			
	sabre	toqm	bqskit	canop	sabre	toqm	bqskit	canop	sabre	toqm	bqskit	canop	sabre	toqm	bqskit	canop	sabre	toqm	bqskit	canop	sabre	toqm	bqskit	canop
bigadd	1.90	1.48	1.28	1.33	1.74	1.32	1.04	1.16	2.00	1.60	1.18	1.46	1.49	1.16	1.01	1.04	1.55	1.23	1.14	1.09	1.51	1.17	0.98	1.01
bv	2.44	1.89	3.00	1.56	2.44	1.89	3.00	1.61	2.46	2.04	2.83	1.50	2.00	1.58	2.42	1.22	1.92	1.53	2.22	1.25	2.04	1.61	2.36	1.22
ising	1.00	1.00	8.00	1.00	0.46	0.46	6.75	0.46	0.75	0.75	4.31	0.75	0.46	0.46	2.67	0.46	0.75	0.75	3.62	0.75	0.46	0.46	3.56	0.46
knn	1.98	2.11	1.90	1.39	1.69	1.85	1.48	1.16	1.92	1.96	1.62	1.32	1.41	1.50	1.36	1.01	1.55	1.62	1.52	1.10	1.44	1.53	1.27	1.02
multi	1.86	1.98	1.94	1.57	1.73	1.92	1.48	1.43	1.98	1.99	1.52	1.71	1.48	1.58	1.30	1.28	1.52	1.56	1.55	1.23	1.51	1.61	1.18	1.23
qec9	3.00	3.58	3.67	1.92	3.00	3.58	3.67	1.83	3.06	3.38	3.31	1.81	2.47	2.85	2.71	1.51	2.38	2.71	2.75	1.50	2.52	2.92	2.87	1.62
qft	3.09	2.88	4.41	2.15	2.22	2.32	2.98	1.54	2.32	2.20	3.14	1.57	1.72	1.75	2.11	1.45	2.17	2.02	3.05	1.91	1.78	1.81	2.03	1.37
qpe	2.80	2.50	3.02	2.22	2.10	1.95	2.04	1.61	2.10	1.90	2.16	1.49	1.62	1.49	1.58	1.18	1.95	1.76	2.08	1.46	1.67	1.54	1.62	1.24
qram	2.06	1.83	2.35	1.35	1.88	1.71	1.58	1.28	2.03	1.86	1.83	1.55	1.56	1.42	1.56	1.28	1.63	1.46	1.71	1.21	1.59	1.45	1.34	1.23
sat	1.57	1.55	1.44	1.50	1.41	1.42	1.16	1.32	1.68	1.68	1.22	1.45	1.22	1.22	1.09	1.06	1.30	1.28	1.11	1.20	1.24	1.24	0.86	1.12
swapt	1.97	2.11	1.98	1.39	1.68	1.85	1.23	1.24	1.94	1.96	1.49	1.31	1.41	1.50	1.27	1.05	1.55	1.62	1.54	1.08	1.44	1.53	1.22	1.00
wstate	1.00	1.00	1.36	1.00	1.00	1.00	1.23	1.00	1.50	1.50	1.79	1.50	1.00	1.00	1.85	1.00	1.00	1.00	1.29	1.00	1.00	1.00	1.32	1.00
Avg.	1.94	1.87	2.47	1.49	1.63	1.61	1.94	1.24	1.89	1.81	2.02	1.42	1.39	1.36	1.65	1.09	1.54	1.47	1.83	1.2	1.41	1.38	1.56	1.09